Benha University
Faculty of Engineering at Shoubra
Geomatics Engineering Department

EVALUATING AND IMPROVING THE ACCURACY OF GLOBAL DIGITAL ELEVATION MODELS

A Thesis Submitted in Partial Fulfillment of the Requirements for the M.Sc. Degree in Geomatics Engineering

Submitted By

Eng. Amal Atef Abdel Fattah Morsy Abo-Salim

B.Sc. in Surveying Engineering (2016)

Supervised By:

Prof. Dr. Ahmed Abdel Sattar Shaker
Prof. of Surveying and Geodesy
Faculty of Engineering at Shoubra
Benha University

Prof. Dr. Abdallah Ahmed Saad
Prof. of Surveying and Geodesy
Faculty of Engineering at Shoubra
Benha University

Dr. Shams El-Dean Mohammed Saad
Lecturer of Surveying and Geodesy
Shoubra Faculty of Engineering-Benha University

Cairo – Egypt

2023

كلية الهندسة بشبرا

FACULTY OF ENGINEERING AT SHOUBRA

APPROVAL SHEET

Evaluating and Improving the Accuracy of Global Digital Elevation Models

A Thesis Submitted in Partial Fulfillment of the Requirements for the M.Sc. Degree in Geodesy

Submitted By

Eng. Amal Atef Abdel Fattah Morsy Abo-Salim

B.Sc. in Surveying Engineering (2016)

Examiners committee

Prof. Dr. Ahmed Abdel Sattar Shaker Signature.A.S......

Prof. of Surveying and Geodesy
Faculty of Engineering at Shoubra
Benha University

Prof. Dr. Mahmoud El-Noqrashi Othman Signature.........

Prof. of Surveying and Photogrammetry
Faculty of Engineering
Al-Azhar University

Prof. Dr. Saad Zaki Bolbol Signature.........

Prof. of Surveying and Geodesy
Faculty of Engineering at Shoubra
Benha University

Prof. Dr. Abdallah Ahmed Saad Signature A A Saad

Prof. of Surveying and Geodesy
Faculty of Engineering at Shoubra
Benha University

Date 19/09/2023

كلية الهندسة بشبرا

FACULTY OF ENGINEERING AT SHOUBRA

APPROVAL SHEET

Evaluating and Improving the Accuracy of Global Digital Elevation Models

A Thesis Submitted in Partial Fulfillment of the Requirements for the M.Sc. Degree in Geodesy

Submitted By

Eng. Amal Atef Abdel Fattah Morsy Abo-Salim

B.Sc. in Surveying Engineering (2016)

Supervision committee

Prof. Dr. Ahmed Abdel Sattar Shaker Signature A. Shaker

Prof. of Surveying and Geodesy
Faculty of Engineering at Shoubra
Benha University

Prof. Dr. Abdallah Ahmed Saad Signature A.A. Saad

Prof. of Surveying and Geodesy
Faculty of Engineering at Shoubra
Benha University

Dr. Shams-Eldean Mohammed Saad Signature Sum

Lecturer of Surveying and Geodesy
Faculty of Engineering at Shoubra
Benha University

Date 19/09/2023

Dedication

This thesis is dedicated for the sake of Allah, my creator, my master and my great teacher. I dedicate this work to my parents, my daughter Nour and my son Anas for their endless support and love.

Amal Atef

Abstract

Representing the earth surface topography is necessary in many applications and uses. Long time and great efforts are needed to make this by the traditional ground instruments. The revolution of satellite mapping enabled obtaining Digital Elevation Models (DEMs) to wide areas of the earth surface. So, the representation of the earth surface became easy and saves time and effort. Unfortunately, the biggest problem of this way is the low accuracy of these DEMs in many places according to the nature of the earth surface and the absence of the data in other places (voids). So, the need to evaluate and enhance the performance and accuracy of these DEMs become necessary.

In this study, the accuracy of two global digital elevation models: Shuttle Radar Topography Mission (SRTM1) and ALOS-PALSAR (ALOS Phased Array type L-band Synthetic Aperture Radar) are evaluated by using ground orthometric and GPS heights. Data in two different test areas are used: A grid of 239 fixed points cover an area of 18.85 by 12.15 km in Toshka south of Egypt, about 55,000 Feddans and a grid of 2722 points in the southwest of Egypt cover an area of 210 by 120 km, about 6 million Feddans.

The evaluation process was made by comparing the ellipsoidal heights of the two sites points with their corresponding values in the used two DEMs and also comparing the orthometric heights of the first site points with their corresponding values in two DEMs.

Then enhancement process made by through four steps. The first step is converting the ellipsoidal heights of the used DEM to orthometric values by

using (SGG-UGM 2) global geoid model instead of the used EGM96 to show the effect of undulation values on the DEMs values. This process was applied to the two DEMs in the first site (Toshka south of Egypt). The second step is shifting the model heights using one point in the middle of the area, where the value of this shift is the difference between the ground value and its corresponding value on the used DEM. This shift process is applied on the orthometric height values (in the first site) and once more on the ellipsoidal height values (in both areas). The third step is shifting using well distributed five points while, every point served an area with 4km radius, this method was made in two sites included in test area 2. The fourth step is applying first and second order polynomials by using the well-distributed five and seven control points respectively (in both test areas). Again, the shift process is applied on the orthometric height values (in the first site) and once more on the ellipsoidal height values (in both sites) using the well distributed five points. The obtained results showed that in most study cases SRTM1and ALOS-PALSAR both gave reasonable results for the geodetic heights and it is better to deal with the ellipsoidal heights of the GDEMs and they showed also that shifting process using one point is the best improving method among the other methods applied in this thesis.

Acknowledgements

I would like to express my gratitude to my supervisors, Prof. Dr. Ahmed Abdel Sattar Shaker, Prof. Dr. Abdallah Ahmed Saad, and Dr. Shams El-Dean Mohammed Saad, for their guidance, support, and encouragement throughout my research. Also I extend my sincere thanks to Dr. Ahmed Abdel-Hai for his moral support.

TABLE OF CONTENTS

LIST OF TABLES

TABLE OF FIGURES

CHAPTER ONE

INTRODUCTION

CHAPTER 1: INTRODUCTION

1.1 Motivation

Digital elevation models are essential for many applications, including hydrology, land use, landslide monitoring, development of dam areas and drainage channel networks and others. Some of these applications demand great precision from DEM in addition to saving the expenses. Global Digital Elevation Models (GDEMs) are beneficial in covering most of the earth's surface but they are neither accurate nor precise to the most required limits. Also, the majority of the world's regions do not have openly accessible high resolution DEMs smaller than 30m. Users are using those GDEMs which is misleading in some applications. Trusted data from ground surveying (e.g., level, theodolite, total station, GPS, and laser scanner) can be added to the GDEM to improve its precision and accuracy and enhance its resolution. In the absence of ground data for enhancing the DEM, simple suggestions could be introduced to the users for improving the performance of the used DEM. This is the motivation behind this thesis.

1.2 Problem Statement

Many applications require the representation of the earth's surface. Using ground-based surveying instruments would take time and effort, but the revolution of satellite mapping, made it possible to obtain digital elevation models of large portions of the earth's surface. The portrayal of the earth's surface is now simple and time and effort efficient. Unfortunately, the major issue with this approach is the low accuracy and precision of these DEMs in many locations due to the characteristics of the earth's topography and the lack of data in other locations (voids). Before using them, their accuracy and precision should be assessed, and their performance should be improved.

1.3 Objectives

The primary objectives of this research are:

1- Studying the Global Digital Elevation Models, their establishment, data sources, mathematical models, and error sources.
2- Studying the prediction methods and the methods of improving the accuracies of the Digital Elevation Models.
3- Investigating the accuracies of some common Global Digital Elevation Models (GDEMs) using terrestrial observations.
4- Proposing and executing some simple methods for improving the performance of the Global Digital Elevation Models.

1.4 Previous Studies

Droj (2008) claimed that a high density of known points and the Delauney algorithm can improve the Digital Terrain Models (DTM's) quality. For the Delaunay triangulation method of computation, each hill or valley must have at least three points. She compared the various algorithms used to generate a DTM, identified the variables that affect the DTM's accuracy and enhanced the resulting DTM's quality. For the first DTM, spot elevations were measured using photogrammetry on an orthorectified airborne image of the region. The end result of aerial laser scanning or close-range photogrammetry data collecting is a dense array of dots with three coordinates (x, y, and z). Computing the TIN model of these points allowed for the fast creation of a DTM. ARCGIS Desktop 9.1 was used to create the area's Triangulated Irregular Network (TIN). This model will act as the reference for comparing and contrasting the most widely utilized interpolation techniques for DTM production. These techniques include Nearest Neighbors - Voronoi diagrams, Inverse Distance Weighted (IDW), Spline Biquadratic, Spline Bicubic, B-spline, Delaunay Triangulation, Quadratic Shepard, and Kriging interpolation. The first phase involved making a regular grid with a step of 500 meters, which resulted in a total of 30 points. The second step involved making a regular grid with a step of 250 meters, which resulted in a total of 121 points. Algorithms were evaluated on this set of criteria.

The findings from the two scenarios demonstrate that the algorithms for Kriging, Shepard, and B-spline in the first case (grid of 500 m), and Delauney triangulation in the second case (grid of 250 m), followed by Shepard and Kriging, produce the most accurate surfaces.

Arefi and Reinartz (2011) presented a method for improving the quality of Advanced Spaceborne Thermal Emission and Reflection Radiometer (ASTER) GDEM data, by employing ICESat (Ice, Cloud, and land Elevation Satellite) laser altimetry data as Ground Control Points (GCPs) to rectify systematic height inaccuracies and a segment-based outlier detection and elimination algorithm to remove artifacts and anomalies. A water mask created from a high-resolution shoreline data set is also used to correct elevation problems within water bodies. The results showed that the updated ASTER GDEM is much more accurate and that the majority of artifacts have been correctly removed. However, due to confusion with some actual non-terrain 3D objects, artifacts with lower height values in relation to the nearby ground pixels are not completely erased. The suggested approach is especially beneficial in regions without access to other high-quality DEMs like Shuttle Radar Topography Mission (SRTM).

Isioye et al. (2011) employed three different spatial data sources (SRTM 30, Digitized Topographical map, and Google Earth Pro) to create a DEM and compared them to field recorded data from a Total Station Instrument. Four hundred ninety-five radial points over the test site were used to create a digital elevation model using the field data. Statistically, the resulting DEM's accuracy was evaluated by comparing;

(1) predictions of some topographic characteristics (slope and aspect),

(2) overall performance of spot height estimates and,

(3) a field measurement's height scale and spot estimation errors' independence.

The results showed that the satellite imagery's DEM (SRTM 30) performs poorly when used to gather data for topographic works. Although the digitized topographic map produces good results, the variance from the reference in this study may be due to human activities, erosion that has taken place since the topographic map was developed, as well as the topographic map's quality. It was also determined that the Google Earth Pro performed significantly better than the SRTM 30 data. Finally, it was suggested that SRTM data and other global terrain data sources, such as GTOPO, be verified for speed and accuracy using Real Time Kinematic GPS in combination with a total station.

Mukherjee et al. (2013) used high-posting Cartography Satellite (Cartosat) DEM and Survey of India (SOI) height data to evaluate open source DEMs (ASTER and SRTM) and their related properties.

When compared to the Cartosat DEM, the overall vertical accuracy for ASTER and SRTM DEM displays RMS errors of 12.62 m and 17.76 m, respectively.

Ouerghi et al. (2015) validate two near-global DEMs, SRTM and ASTER-GDEM, with a reference DEM used on the SW of Grombalia in North-East Tunisia. A 1:25,000 topographical map created by the Office of Topography and Cartography of Tunisia served as the basis for the reference DEM. Some of the techniques used in the comparison include DEM differencing, profiling, correlation plots, extraction of catchment areas and drainage networks, and computing of Horton statistics.

According to the findings, SRTM has better vertical accuracy (measured in terms of RMSE) than ASTER-GDEM for the chosen site. For SRTM and Advanced Spaceborne Thermal Emission and Reflection Radiometer (ASTER), the RMSEs varied from 7.62 to 10.53 meters, respectively. Thus, in flat and less complicated terrain, the vertical accuracy of both products improves.

Amin et al. (2013) concluded that a comparison between the local DEM derived from 1:50,000 scale topographic maps based on a rectangular grid and the ASTER and SRTM global DEMs can be used to assess the evaluation procedure. In order to complete the evaluation procedure, a total of 705 GCPs were made accessible in the northern Nile valley, which was designated as the study area. This area's boundaries are (30° to 31.5°) of longitude and (28° to 31.5°) of latitude.

The findings demonstrate that ASTER DEM is ranked last whereas SRTM and the local DEMs are comparable to one another in terms of RMSE.

Additionally, the outcomes revealed a 12.55 m downward slope (average shift between the GCPs and ASTER DEM). After eliminating this shift, this DEM's vertical accuracy was significantly improved by 57.8% over steep terrain and 48.8% over flat terrain, leading to the conclusion that the SRTM DEM can be used to update topographic maps at a scale of 1:50,000 because its accuracy was found to be less than half the contour interval of such maps. The ASTER DEM can also be used for the same purpose, but for smaller-scale maps, by removing its vertical shift (vertical systematic errors).

Elsayed and Ali (2016) used the polynomial model and cubic convention resampling to modify the methodology based on merging the GPS ground control points with the SRTM surface. This polynomial model is examined using a variety of data points and various data point spacings. There are four basic approaches, each with a different point spacing. For two example studies, the spacing is 500, 375, 250, and 125 metres (flat and semi-flat areas).

The following can be derived from the findings:

- Resampling improved the outcomes for the initial SRTM, but it had no impact on the statistics values for the various solutions once the polynomial was applied.
- The polynomial of first order with an average separation of 250 m produced the best results.
- In comparison to used GPS checkpoints, the best vertical accuracy's RMSE for flat and semi-flat terrain is 0.42 m and 1.21 m, respectively.

Hussein (2016) compared the accuracy of a digital elevation model (DEM) made using a portable GPS to a version 2 of the Advanced Spaceborne Thermal Emission and Reflection Radiometer Global Digital Elevation Model (ASTER GDEM). For the purpose of creating and analyzing the resulting DEM, the University of Baghdad's Al Jadriya campus was chosen as the research location. Additionally, GPS track points (elevation data) of the study region were visualized, analyzed, and extrapolated using a Geographic Information System (GIS). In order to determine the impact of the number of points included on the accuracy of the resulting DEM, three additional DEMs were constructed in this study using 60%, 30%, and 15% of the total GPS track points, respectively. When all GPS tracking points that were observed throughout this research were taken into account.

The study results reveal a high resolution for the resulting DEM less than 5m. Additionally, the generated DEM has relative precision that is superior to absolute accuracy and is around 2m. Comparing handheld GPS DEM quality to ASTER GDEM, ground control points (reference points) demonstrate a significant improvement. Thus, this study suggests that doubling the observed number of GPS track points will increase the accuracy level of a portable GPS DEM by roughly 40%.

Dawood and Al-Khamdi (2017) have investigated the accuracy of eight GDEMs including the EarthEnv-D90, SRTM 1, SRTM 3, ASTER, GMTED2010, GLOBE, GTOPO30, and AW3D30 in two study locations in Egypt and Saudi Arabia that represent various topographic patterns. The performance of such DEMs has been assessed using well-known ground control points with precisely determined coordinates and elevations. The range, standard deviation, correlation, kurtosis, and skewness of five statistical metrics have been independently assessed for each DEM's mistakes. The concept of the weighted average is then used to create a new reliability index.

The obtained results demonstrate that global DEMs behave differently under various topographic patterns. It has been determined that the EarthEnv-D90 and SRTM1 models achieve high dependability indices in the Nile delta region, which represents flat terrain, whereas the GMTED2010 and EarthEnv-DEM90 models take first position for the second study area, Makkah, which represents mountainous topography.

According to their findings, these GDEM models provide standard deviations of height differences that range from 4.7 to 18.6 meters in mountainous locations and between 2.0 and 6.7 meters in flat regions.

Rabah et al. (2017) investigated a number of GDEMs (ASTER, SRTM1 and SRTM3) in Egypt. 601 points of observed ellipsoidal heights have been compared with the three GDEMs. The results showed that the SRTM1 is the most accurate one, producing a mean height difference of ±2.89 m and standard deviations of ±8.65 m, respectively.

To enhance the accuracy of GDEMs, they used the GECO global geoid model to get the orthometric heights, and then two orthometric height models (SRTM1 ellipsoidal height + EGM96) and (SRTM1 ellipsoidal height + GECO) were assessed with 17 GPS/levelling stations and 112 orthometric height stations.

The results showed that the estimated height differences between the SRTM1 before improvements and the enhanced model are 0.44 m and 0.06 m, respectively.

Yang et al. (2018) stated that GNSS measurements are used to calibrate the ASTER GDEM2 by simple and multiple linear regression analysis. ASTER GDEM2 can be enhanced by either calibration technique. The impact of land use on elevation error is solely taken into account by the simple linear regression approach, whereas both topographical and land-use aspects are taken into account by the multiple linear regression method. The simple linear regression calibration approach is straightforward and simple to implement, as opposed to the multiple linear regression calibration method, which calls for additional data input during modeling. It opens up the possibility of calibrating ASTER GDEM datasets for regions that have comprehensive land-use information and accurate field-based elevation measurements. High-resolution satellite remote sensing photography can be used to derive precise land-use information in situations where there are no such data.

Jalal et al. (2020) used a watershed map, and three extracted GDEMs, SRTM DEM, ALOS PALSAR DEM, and TanDEM-X with different resolutions are validated based on the RMSE, outlier identification, and the quantity of extracted stream orders. The handheld GPS locations' derived DEMs actually perform better than the GDEMs when outliers are taken into account. The GCPs were used to validate the vertical accuracy (heights) of the GDEMs.

The findings showed that the TanDEM-X, ALOS PALSAR, and SRTM DEM height differences, as well as their corresponding root mean square errors (RMSEs), indicate 7.3 m, 7.6 m, and 6.5 m, respectively.

Liu et al. (2020) evaluate the quality of five global DEM datasets (SRTM-1 DEM, SRTM-3 DEM, ASTER GDEM2, AW3D30 DEM, TanDEM-X 90-m

DEM) and one 30-m resampled TanDEM-X DEM) over the Hunan province in south-central China. The accuracy of these DEMs is then assessed using the recently released high-precision ICESat-2 (Ice, Cloud, and Land Elevation Satellite-2) altimetry points.

The results showed that the ASTER GDEM2 has the worst quality, with an RMSE of 10.1 m, and the SRTM1 DEM provides the best quality, with an RMSE of 8.0 m.

Dawood and Amin (2022) stated that the vertical accuracy of global digital elevation models can be improved by including terrestrial GPS data and using two methods in the enhancement process: the regression modelling method and the kriging geostatistical method.

Based on the available datasets and obtained results, it has been found that the regression modelling method improves the vertical accuracy of the investigated two GDEMs by 15% and 4% while 24% and 16% improvements obtained by the kriging geostatistical method.

El-Ashmawy and Al-Karagy (2022) employed the proposed empirical surface subtraction approach and the linear regression analysis approach to assess and enhance the vertical accuracy of the three global digital elevation models: SRTM, ASTER, and ALOS (AW3D30). Only 980 of the 1,042 GPS/leveling points in Egypt that were available for use were used because the outlier points based on 3σ were also extracted. From the remaining spots, 390 checkpoints and 500 control points were created. The 390 check points are used to assess the three global DEMs. The outcomes are reflected in the table (1.1).

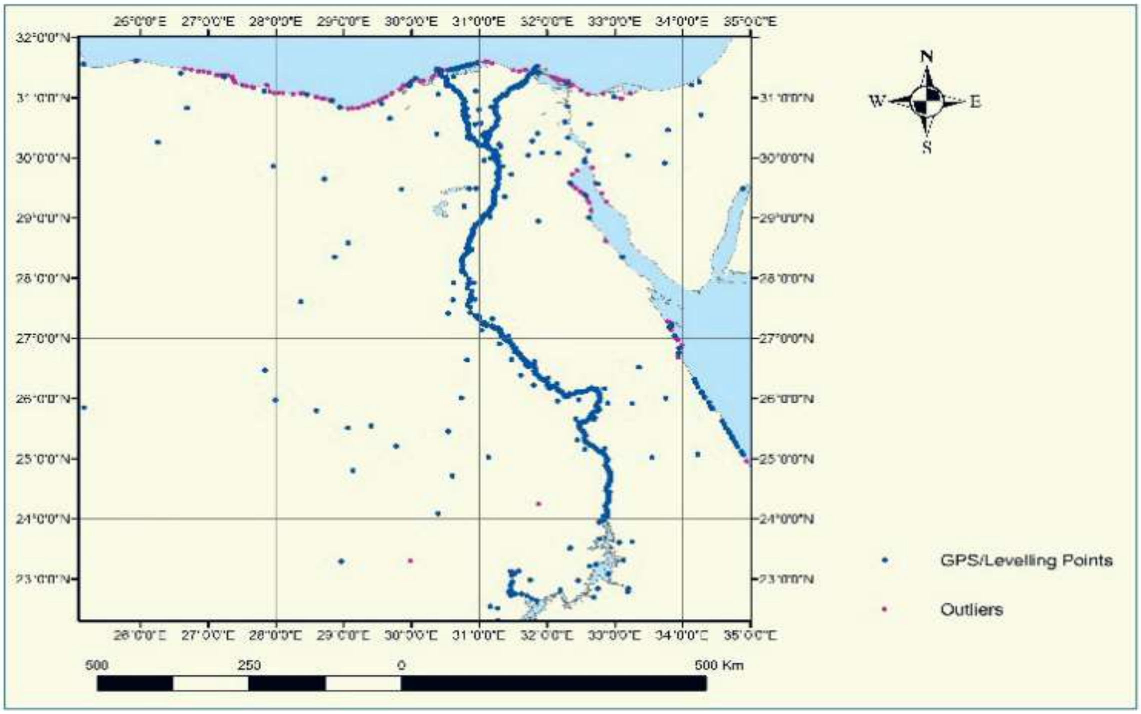

Figure 1.1. The location of the extracted outlier data and the remaining points, after **(El-ashmawy and Al-Karagy, 2022).**

Table 1.1. the results of the tested three models, after **(ibid).**

	(SRTM) m	**(ASTER) m**	**(AW3D30) m**
Max	12.38	43.04	11.45
Mean	1.30	3.54	-0.02
Min	-12.81	-19.95	-7.53
RMSE	3.99	8.81	2.98

1.5 Thesis Structure

This thesis provides an explanation of the different types of digital models, their data sources, their resolution and accuracy, interpolation techniques, and various techniques to assess and improve the performance of widely used global digital elevation models. Five chapters make up this thesis.

In Chapter 1, motivation, problem statement, objectives, previous studies, and an overview of thesis structure are introduced.

In Chapter 2, the three digital models, surface, elevation, and terrain are defined. The DEMs' applications are then stated. The chapter also describes the DEMS' resolution and accuracy. The different data sources required to create a DEM are illustrated. Finally, some of the satellite missions that were used in creating DEMs and the resulting global models are described.

In Chapter 3, the various interpolation-related topics are covered. It describes the interpolation procedure, lists the different interpolation methods, and describes the different forms of spatial interpolation. There is an explanation of the various DEM creation techniques. Along with the evaluation of the DEMs' correctness, the role of interpolation techniques in particular augmentation of DEMs is presented.

In Chapter 4, the data that were used and the methodology that was employed are briefly described to support the research's objectives. The obtained results and their analysis are illustrated in the chapter.

In Chapter 5, a summary of the subject and the conclusions for assessing and improving the performance of the global digital elevation models were offered.

This chapter also includes some recommendations for additional future research and final comments.

CHAPTER TWO

DIGITAL ELEVATION MODELS

CHAPTER 2: DIGITAL ELEVATION MODELS

This chapter includes definitions of the three digital models, surface, elevation, and terrain. Then the uses of the DEMs are stated. The chapter also defines the resolution and the accuracy of the DEMs. The different data sources needed to build a DEM are illustrated. Finally, some of the used satellite missions and their resulted elevation models are described.

2.1 Definitions

Digital Elevation Model (DEM): is a representation of the earth surface topography in three dimensions in the form of digital image where each pixel contains a value which represents the elevation value of the center of the pixel and can be derived from topographic maps or photogrammetric and remote sensing methods. Additionally, it is a digital representation of the elevation of the land's surface in relation to any reference datum **(Balasubramanian, 2017)**.

The earth surface can be represented by three models:

- **Digital Surface Model (DSM):** The tops of buildings, trees, vegetation, powerlines, and any other items picked up by the sensing technique are all included in digital surface models. These are helpful for designing cities and for simulating the landscape.
- **Digital Elevation Model (DEM):** A three-dimensional, computer-generated representation of a terrain surface is called a digital elevation model. A DEM, often known as a "bare-earth" elevation model, is devoid of all vegetation, buildings, and other non-terrain

items.DEMs can be seen as either a triangular irregular network (TIN) or a grid of squares (https://geodetics.com/dem-dsm-dtm-digital-elevation-models), see figure 2.1.

- **Digital Terrain Model (DTM):** is the representation of the earth surface without any features (natural and humane made) by including vector features of the natural terrain, such as rivers and ridges (ibid).

The DEM is generated by making an interpolation to the DTM but not vice versa.

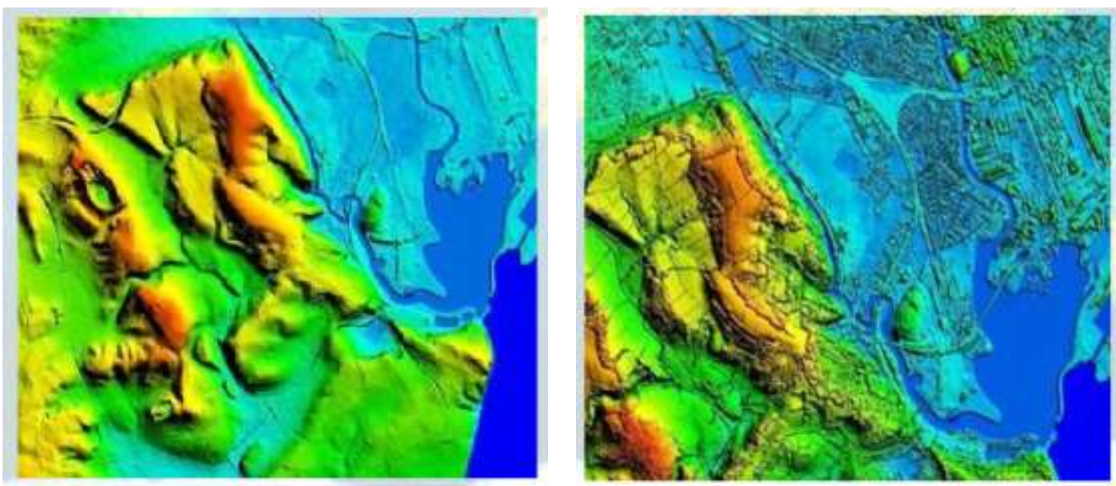

DTM DSM

Figure 2.1. Digital Terrain Model against Digital Surface Model, after **(https://en.unesco.org/sites/default/files/ukzn_dem_lecture_for_uploa).**

2.2 Uses of DEM

Digital Elevation Models (DEMs) are essential for a variety of geomatics applications, including determining flood hazard and using them for geomorphologic watershed management. The importance of DEMs in geodetic applications is very significant **(Mirza et al., 2011)**.

a) **Water Resources Management:** Accurate elevation data are needed to Water Resource Management (WRM) including its branches where the shape of the earth determines the water flow direction. The main goal of water resource management models is to use water resources as efficiently as possible to satisfy the needs of many users as possible, **(Islam, 2011)**.

b) **Water Catchment (watershed) Mapping:** A watershed is a region of land where all of the water that accumulates there and drains away from it empties into a single location. A physical divide, such as a ridge or a crest, between two or more contiguous catchment basins also serves to define a watershed.

   Watershed analysis describes the method of defining watersheds and obtaining properties such as streams, stream networks, catchment regions, basins, etc. using raster and DEM data.

   A watershed generally has five parts: the watershed boundary, the subbasin, the drainage divides, the stream network, and the outlets (pour points), (https://gisresources.com/giswatershedwatershed-analysis), see figure 2.2.

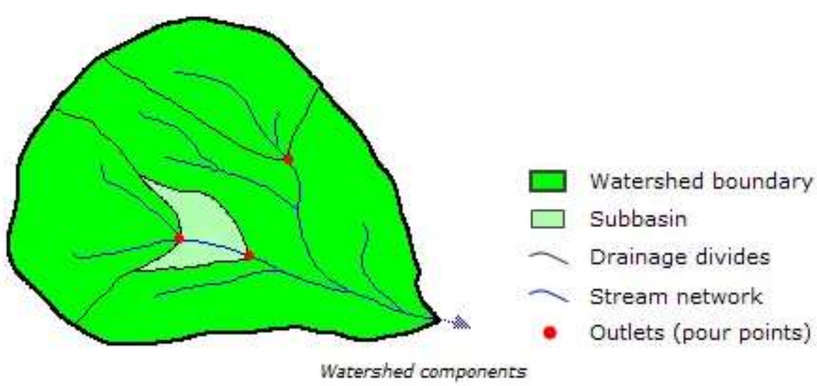

Figure 2.2. watershed components, after **(ibid).**

Where:

Subbasin: A larger watershed that is also capable of containing smaller watersheds.

Drainage divides: Drainage divides are the lines dividing one watershed from another.

Outlets: The point on the surface at which water pours out of a space is known as the outlet or pour point. It is located at the watershed's lowest point.

c) **Bathymetric Analysis (depth maps):** Bathymetric analysis, also known as water depth analysis, is crucial for applications in a variety of fields, including ecology (submerged morphology, such as the structure of the seafloor), traffic and transportation (harbors, landing zones), disaster modelling and response (wave action, tsunami impacts), monitoring and mitigation of beach erosion, and more. Thus, water resource management and coastal monitoring are frequently combined with bathymetric investigations, (https://pubs.usgs.gov/tm/11b4/pdf/tm11-B4.pdf).

d) **Disaster Risk Management(DRM): DRM** For mapping and evaluating disaster risks as well as for preventing, detecting, and responding to disasters, three-dimensional (3D) data are crucial. For instance, it is becoming more common to forecast, map, and manage storm and other natural catastrophe events using terrain modelling and surveying for both exposed and below-water topographies, (ibid)

DEMs are essential for DRM in domains like:

- Disaster hazards connected to elevation. For instance, elevation is directly related to the hazards of disasters like floods, coastal erosion, storms, and/or tidal waves.

- Building structural deterioration. The best way to assess structural damage at the level of detail required for effective disaster response when the type of building damage is not visible in aerial or satellite photography is using 3D Lidar data.
- Because vegetation height (fire fuel load) is determined by removing the top-most height surface from the DEM, wildfire hazards are linked to elevation data. Furthermore, a trait that is also obtained from DEMs is the assumption made by fire models that upslope fire propagation speeds increase.

e) **Floodplain Management**: A technique for preserving and respecting the floodplain, **(Nagarajan et al., 2022)**, DEMs are necessary for (i) creating flood risk maps, (ii) creating flood hazard models, (iii) assessing flood response plans, and (iv) creating floodplain management plans, (https://pubs.usgs.gov/tm/11b4/pdf/tm11-B4.pdf).

f) **Geological Applications:** DEMs are used extensively in the domains of geophysics, geomorphology, and geology. Landform, geohazard mapping based on shaded relief maps that reveal information about, for example, illumination angles, contour maps, aspect maps, or slope maps, are a few examples of the geologic uses, (ibid).

g) **Coastal Monitoring:** Because of advancements in mapping and monitoring technology as well as for determining the effects of coastal climate change, DEMs are being employed more and more for coastal applications. DEMs play a key role in defining the following in coastal monitoring: Shoreline delineation, Sea level rise, Coastal management, Coastal engineering, Coastal flooding, and Underwater applications.

h) **Urban Analysis:** The use of DEMs in urban study includes choosing an appropriate location for a development;

  - Evaluating drainage infrastructure and patterns in urban environments.
  - Making plans for lush landscapes.
  - Evaluating the state of the infrastructure (roads, bridges, etc.).

i) **3D Visualization:** More varied applications range from creating 3D city and landscapes for the gaming or entertainment industries to creating precise 3D environmental models for simulation needs.

j) **Mapping:** the geographic information system that is now used to create smart maps in the form of layers, each layer containing a feature such as:

  - Point layer contains point features such as towns.
  - Line layer elements like rivers and highways are contained within it.
  - The DEM layer is significant for the third dimension and incorporates polygon characteristics such as city boundaries.

k) **Planimetric Maps:** show the horizontal (x, y) positioning of landscape elements. In order to show horizontal features in their precise horizontal locations, this type of mapping requires the use of elevation data, such as from a DEM. This is especially true for maps made from stereo imagery, when tall things are more widely spaced.

l) **Topographic Maps:** The DEM data are required for developing topographic map information since the topographic maps contain all the characteristics seen on planimetric maps but also contain contour and/or spot height information.

2.3 DEM Resolution and Accuracy

Resolution is the smallest horizontal distance at which a satellite may detect an object. Earth's geography determines the minimum geographical distance that the satellite must travel in order to collect data, with moderate relief requiring a large spatial distance and rugged terrain requiring a small spatial distance.

2.3.1 The (Ground-Sample Distance (GSD)): is the density at which Interferometric Synthetic Aperture Radar (IfSAR) or Light Detection and Ranging (LiDAR) devices acquire elevation samples. The minimum size of the terrain features to be detected and the distance between them should be less than the GSD provided for a collection system.

2.3.2 Vertical Accuracy: is the primary quality measure for DEM products. It was obtained by subtracting the elevations measured by ground systems from the DEM elevations.

- It identifies the appropriate application for using DEM.
- Small elevational differences can have big effects on the outcomes.
- The vertical accuracy requirement dominates the control over horizontal accuracy (high vertical accuracy requires high horizontal accuracy).

Two measures of a DEM's quality are the absolute accuracy of elevation at each pixel and the accuracy of the morphology shown (relative accuracy). Comparing DEMs from different sources allows one to gauge a DEM's level of quality. The following factors are significant for the quality of products obtained from DEM (https://www.nasa.gov/missions):

- Terrain roughness,
- Sampling density (elevation data collection method),
- Grid resolution or pixel size,
- Interpolation algorithm,
- Vertical resolution,
- Terrain analysis algorithm.

2.4 DEM Data Sources

The DEM can be produced using a variety of data sources, including conventional ground-based methods, GNSS, radar, geographic data, lidar, field measurements, existing topographic maps, and photogrammetry techniques.

2.4.1 Traditional Ground-based Methods (Tachymetry-based field surveying provides terrain heights at specific sites.): are mainly restricted to small areas yet accurate but time-consuming. Terrain heights are delivered at specific sites via field surveying based on tachymetry.

2.4.2 Satellite Surveying Techniques provide terrain heights along profiles or in various areas (e.g., roads). GNSS is also used to evaluate the height accuracy of DEMs.

2.4.3 Digitizing Contour Lines from Topographic Maps (Hirt, 2015).

In order to create a DEM from an existing topographic map, the elevation contours must be digitized and transformed into xyz data (http://www.terrainmap.com/rm19.html).

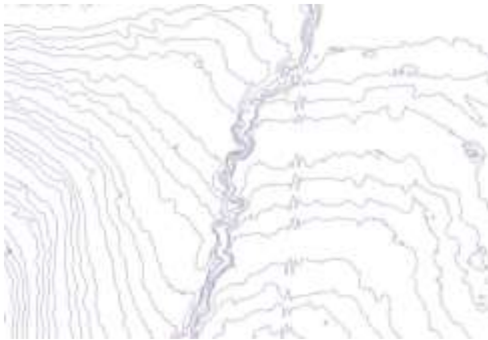

Topographic map

DEM –> Contours

Figure 2.3. DEM representation, after **(https://makoj.com/blog/2018/april/contours-dem/).**

2.4.4 Photogrammetric Methods used two overlapping images taken at two separate locations. Stereoscopic processing can be used to determine the heights of the terrain. Aerial photogrammetry is used nationally, but satellite imagery is used internationally such that (ASTER, SRTM or ALOS satellites). The absence of data in places with cloud cover and vegetation cover is one of these methods' shortcomings.

2.4.5 Laser-based Methods (LiDAR): The laser system calculates the amount of time, it takes for brief laser light pulses to be transmitted, reflected by the earth's surface, and then returned to the system. GPS unit installed on the helicopter or aircraft carrying the measuring equipment. Mirrors are used to distribute waves of laser pulses into swaths in order to sample the covered region with a high spatial resolution. In the vegetation region, when there are two reflected pulses, one from the ground and one from the canopy, it gives information about the height of vegetation and the bare ground.

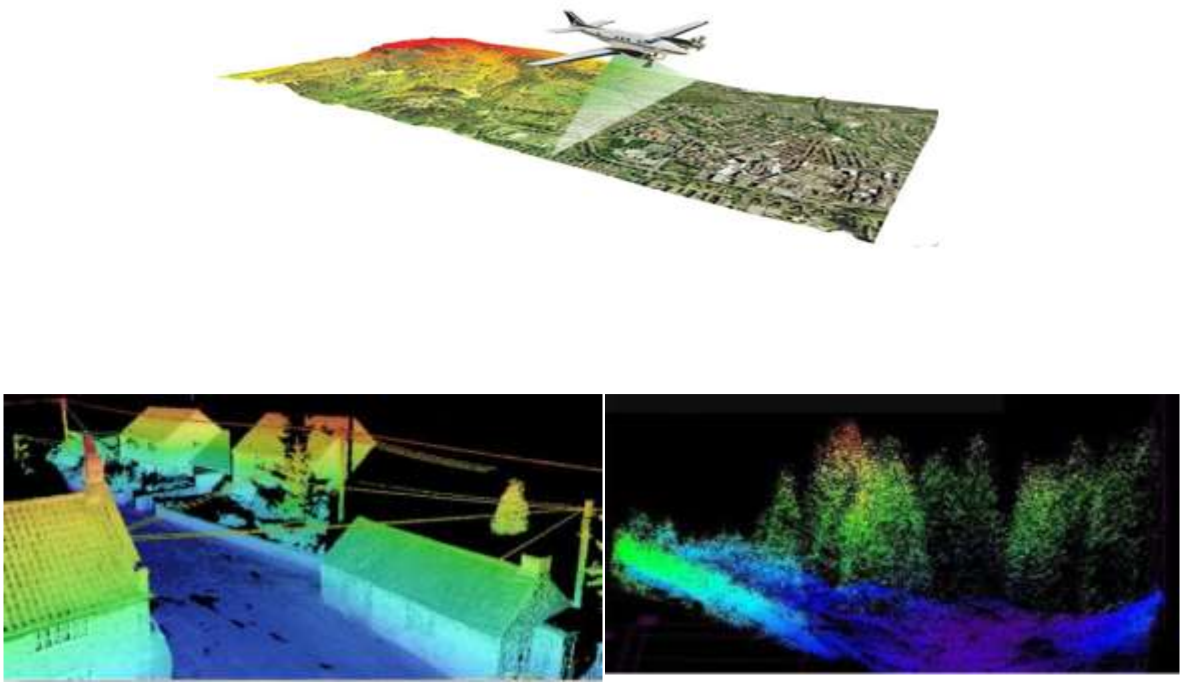

Figure 2.4. Raw LiDAR: Point Cloud, after
(https://en.unesco.org/sites/default/files/ukzn_dem_lecture_for_uploa).

Modern airborne and spaceborne sensors are more valuable than old methods in depicting vast areas because they can gather a lot of data quickly, although classic methods still produce data with high accuracy **(Hirt, 2015).**

2.4.6 Satellite Mapping: Synthetic aperture radar is presently the only sensor technology capable of recording high-resolution image data over a wide region
during both day and night and in all weather conditions (https://www.dlr.de/hr/en/desktopdefault.aspx/tabid-8113/14171_read-35852/).

Radar systems can be used in a variety of frequency ranges. The information that can be obtained from radar imaging depends greatly on the band selection. The frequencies in the L-band have the greatest potential for use in the fields of earth and environmental sciences, according to numerous national and international articles and research in which German experts played a significant role. The L-band, which has a wavelength of 24 cm, is distinguished by having a deep penetration depth for volume scatterers like vegetation, ice, dry soil, and sand. This is in contrast to the shorter wavelengths in the C-band and X-band (wavelengths of 5.6 cm and 3.1 cm, respectively). Thick vegetation can only be penetrated to the ground and measured for vertical structure using long-wave L-band. Long wavelength radar signals also have a significant improvement in temporal coherence, which is crucial for measuring glacier motion and surface deformation (ibid).

Interferometric synthetic aperture radar is a potential method for creating digital elevation models. It uses two passes of a radar satellite (like RADARSAT-1, TerraSAR-X, or Cosmo SkyMed) or a single pass if the satellite has two antennas (like the SRTM instrumentation) to gather enough data to produce a digital elevation map with a resolution of about ten meters. The digital image correlation approach allows for the use of additional stereoscopic pairs by acquiring two optical images from different perspectives during the same flight or pass of an Earth observation satellite (such as the HRS instrument of SPOT5 or the VNIR band of ASTER). Using two-pass stereoscopic correlation, the SPOT 1 satellite (1986) supplied the first useful elevation data for a sizable percentage of the planet's landmass. Later, further data were provided by the Advanced Spaceborne Thermal Emission and Reflection Radiometer (ASTER, 2000) instruments on the Terra satellite, the Shuttle Radar Topography Mission (SRTM), and

the European Remote-Sensing Satellite (ERS, 1991) using variations of the same technique. More than 100 million square kilometers of stereo pairs have been recorded by the
HRS instrument on SPOT5,
(https://en.wikipedia.org/wiki/Digital_elevation_model).

2.4.7 Synthetic aperture radar (SAR) concept: Imaging radar mounted on a moving platform is called synthetic aperture radar. Similar to traditional radar, electromagnetic waves are progressively sent, and the radar antenna collects the backscattered echoes. In the case of SAR, the platform movement causes the consecutive times of transmission and reception to convert into different positions **(Moreira et al., 2013)**.

SRTM using the SAR system to get the heights of ground points as shown in figure 2.5.

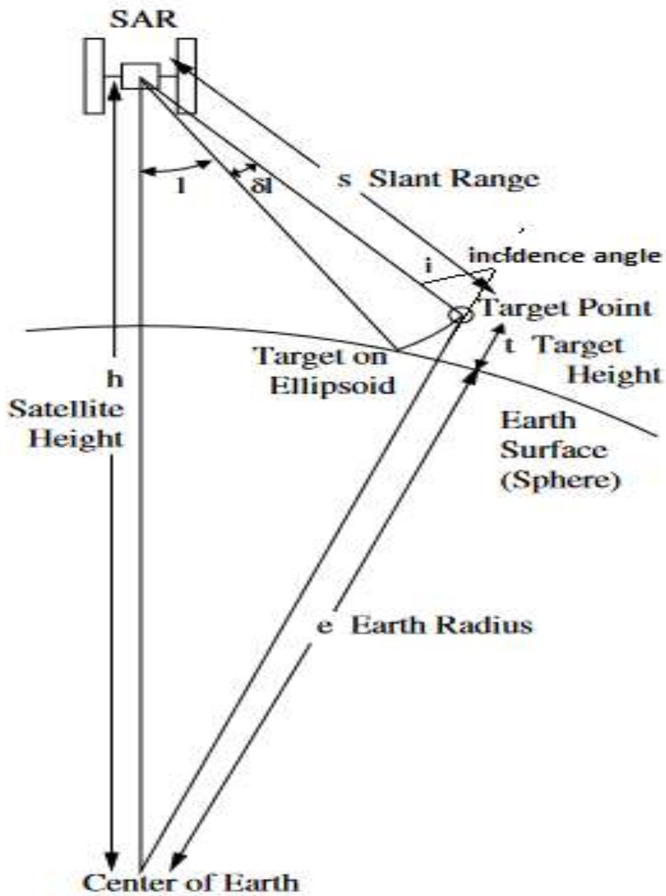

Figure 2.5. A geometrical model for SAR system, after **(https://www.cs.uaf.edu/~olawlor/ref/asf/sar_equations_2006_08_17.pdf).**

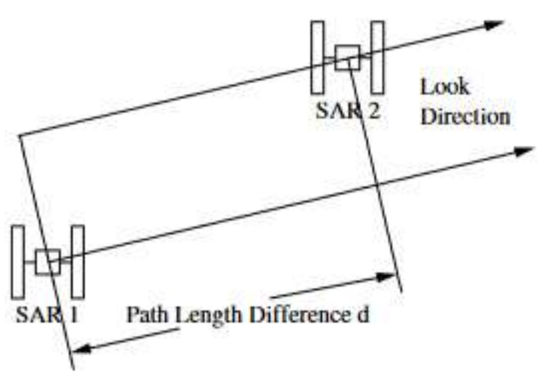

Figure 2.6. Path length difference between the two antennas, after **(ibid).**

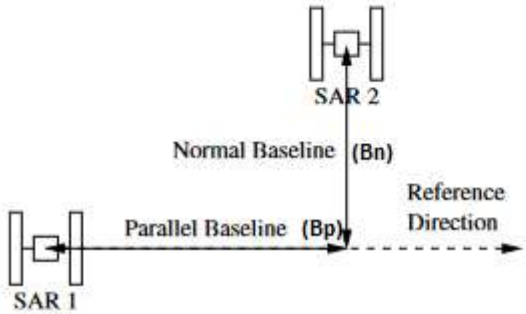

Figure 2.7. Parallel and normal baseline, after **(ibid).**

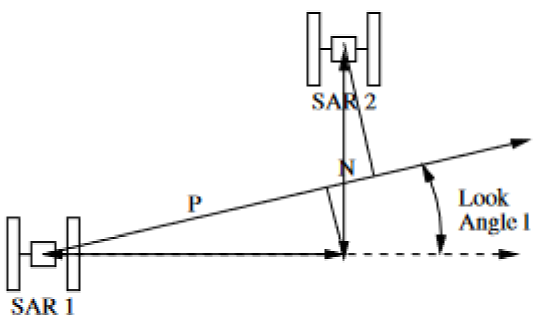

Figure 2.8. Look angle (l), after **(ibid).**

The equation that was used to get the height is as follow **(ibid)**:

$$t = \delta p \frac{s \sin(i)}{2k(-B_p \sin(l) + B_n \cos(l))} \quad (2.1)$$

Where:

- t Topography height above a hypothetical spherical Earth of radius e, meters.
- s Slant range; distance from satellite to target, meters.

- p Phase difference: measured by subtracting the phase of the images to be interfered, radians.
- k Wavenumber; phase change per unit distance, radians per meter. $k = 2\pi/\lambda$, where λ is the radar wavelength in air.
- i Incidence angle; angle from straight up over to satellite, as measured from the target point, radians.
- *l* Look angle: angle from straight down over to target, as measured from the satellite, radians.
- Bp Parallel baseline; distance between satellites measured along the reference direction, meters.
- Bn Normal baseline; distance between satellites measured across the reference direction, meters
- d Distance target moved between observations, projected into the satellite average line of sight, meters. $d = p/2k$
- e Earth radius; distance from center of earth to local ellipsoid, meters
- h Height of satellite; distance from satellite to center of Earth, meters. Can be computed from the state vector XYZ position as $h = \sqrt{x^2 + y^2 + z^2}$.

2.5 Used Satellite Missions and Resulted DEMs

2.5.1 Shuttle Radar Topography Mission (SRTM)

The National Geospatial-Intelligence Agency (NGA) and the National Aeronautics and Space Administration (NASA) cooperated and produced Shuttle Radar Topography Mission (SRTM). SRTM was launched in February 2000 and moved in orbit with inclination angle of 57 degrees. The covered area by SRTM is 80% of the land math of the earth and lie between

60 degrees north and 56 degrees south latitude. The objective of SRTM mission is to produce digital topographic data for the covered area, the produced SRTM digital elevation model has absolute vertical accuracy ±16m. The acquired data by radar system resulted in making more accurate topographic map to the earth surface which hadn't been assembled before, (https://www.usgs.gov/centers/eros).

The gathered data used in military, civil, and scientific purposes, improve the model of water drainage, navigation safety, volcano monitoring, earthquake research, and choose the best location for cell phone towers.

The two radar images taken from two different locations by SRTM hardware consisted of two radar antennas, one of them in the shuttle payload pay and the second attached to the end of a mast far 60 meters away the shuttle.

Radar waves were sent in a beam. Rays from the radar waves that hit the Earth's surface scattered in different directions. The two SRTM antennas gathered these scattered waves.

The outer antenna's baseline distance from the primary antenna was well established and stayed constant. The distance between the Earth's surface and the two antennas did shift. The position within the radar beam that indicates where the reflection occurred varied slightly between the main and outboard antennas.

Accurate elevation of the Earth's surface can be computed using data on the distance between the two antennas and the variations in the reflected radar wave signals.

The Shuttle Radar Topography Mission (SRTM) 1 Arc-Second Global data can be
overview or downloaded from earth explorer,
(https://www.usgs.gov/centers/eros/science/usgs-eros-archive-digital-elevation-shuttle-radar-topography-mission-srtm).

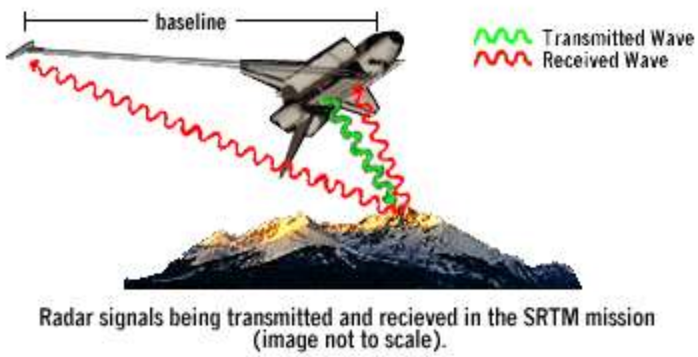

Figure 2.9. Radar signal being transmitted and received in the SRTM mission **(ibid).**

The tool employed is called a Synthetic Aperture Radar (SAR), which uses microwave illumination to create images of the Earth's surface and is therefore unaffected by the position of the sun (time of day), the weather, and the contrast of the surface. High-resolution mapping of the microwave reflectance is mainly owing to the SAR method. In addition to surface imaging, the X-SAR/SRTM system's unique configuration (Figure(2.10)), which includes secondary receiving antennas installed on a 60-meter-long pole to enable an interferometric measurement mode, also enables a measurement of terrain height for determining surface topography **(Hounam and Werner, 1999)**.

The C-band and X-band single pass interferometric SAR equipment is configured by simultaneously running two sets of radar antennas, each having a transmit/receive and a receive-only antenna separated by a baseline and two reception channels. The main transmit and receive (channel one) X-SAR antenna is 12 meters long and 40 centimeters wide, and it is mounted directly to a tiltable portion of the 12 meter C-radar antenna truss structure in the shuttle's cargo bay. In order to create the baseline, the second (receive-only) antenna is installed onto the tip of a 60-meter-long, deployable, stiff boom structure, perpendicular to the space shuttle's direction of motion, together with the second 8-meter-long C-band antenna.

The C-radar can operate in a ScanSAR mode, which would also enable comprehensive coverage of the Earth within the relatively short orbital period of 11 days or 159 orbits, however X-SAR is not capable of doing so. In contrast, X-SAR will work in a higher-resolution mode with a narrower swath width of roughly 50 km that is positioned inside the SIR-C scan swath at an angle of 52 degrees off-nadir.

To line up the secondary antenna's beam with the primary antenna's, the primary antenna may be elevated inclined. By electronically beam steering the receiving antenna in an angle range of 0.9 degrees, the azimuth of both antennas will be aligned in orbit, (ibid).

2.5.1.1 Errors

Inaccuracies in the orbit data, baseline length, tilt angle, and other image geometry factors, as well as phase variances carried on by the instrument, can all contribute to a height error.

As a result of the antennas' spatial separation (baseline), the reflected signals are detected at each antenna with a unique propagation time and phase. The topographic elevation of the location on the Earth's surface that is being reflected is determined by the phase difference between the signals that are being received. Phase offsets caused by systematic inaccuracies in the radar system must be eliminated by calibration.

Although its sweep will be just 50 km wide, the X-SAR will operate in a higher resolution mode. Only about 40% of the surface under observation will be detected. As a result, the lighted swaths of the X-SAR-System choose the locations of the reference target points. The places are situated close to swath crossing spots. Every reference target consequently appears in two distinct SAR pictures in most cases.

It will be necessary to relocate some corner reflectors in between passes. Before a pass, everyone must be facing the shuttle. Additionally, using differential GPS, it is important to determine each corner site's exact location on a map, (ibid).

2.5.1.2 Product

The C- and X-band radar frequencies used in the SRTM mission will produce digital elevation products in a mosaic format. At latitudes greater than approximately 48° North/South, full X-band coverage starts. Between 60° North and 58° South, the terrain will be entirely covered by the C-band radar, with many overlaps at the upper latitudes.

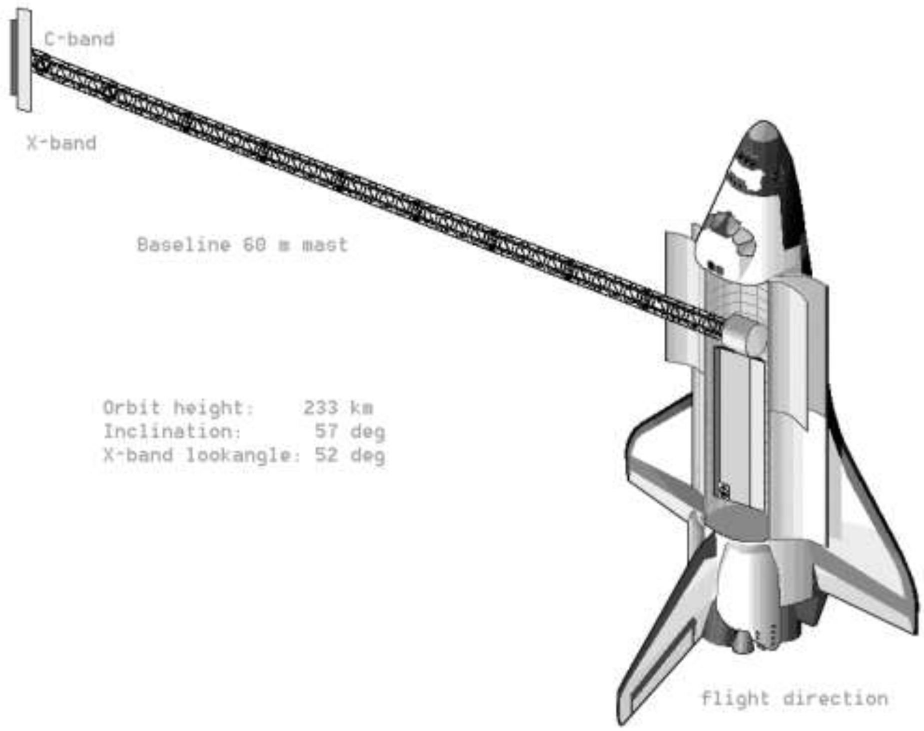

Figure 2.10. Drawing of the SRTM Configuration with the Secondary Antennas mounted on the Mast, after **(ibid).**

Table 2.1. SRTM specifications

Projection	Geographic
Horizontal Datum	WGS84
Vertical Datum	EGM96 (Earth Gravitational Model 1996), WGS84 ellipsoid
Vertical Units	Meters
Spatial Resolution	1 arc-second for global coverage (~30 meters) 3 arc-seconds for global coverage

	(~90 meters)
Raster Size	1 degree tiles
C-band Wavelength	5.6 cm
Global vertical accuracy	±16 m
Resolution	1 arc second, 3 arc second
Generation technique	SAR interferometry
File format	Geo TIFF
Sensor type	Radar (C band and X band)
Spatial extent	60^{o} N to 56^{o} S
Orbit altitude	233 km
Orbit inclination	57^{o}
Mission duration	11 days

2.5.1.3 Shuttle Radar Topography Mission (SRTM) Versions

SRTM 3″ DEMs are available to the public on the Internet, by 1˚x1˚ tiles, published by NASA. Two versions are available: version1(v1) consists of the original data of digital elevation models but these data contain some of untrue data in the areas have low backscattered radar. Version2(v2) was resulted from making enhancement to the data in version 1 by making editing and making well representation to the water bodies and coastlines with the absence of the wells and spikes (single pixel errors). There are areas with missing data is called voids, these areas have snow cover on mountainous areas, (http://www2.jpl.nasa.gov/srtm/). There are a third version (v3) is a part of the two previous two versions with 5˚x5˚ tiles. There are post processing was made to the dataset of NASA data to fill in the data voids by interpolation techniques. There is ½ grid pixel shift between v3 and v2 of SRTM **(Jarvis et al., 2006)**. The error was identified but the direction of it isn't known so another version was prepared (v4) to overcome this shift, **(Mouratidis et al., 2010)**.

SRTM Vertical Accuracy: The absolute vertical accuracy of SRTM global digital elevation model is ±16 m, this vertical accuracy published by Shuttle Radar Topography Mission (SRTM) data specification, **(Elkhrachy, 2018)**.

2.5.2 ALOS-PALSAR (ALOS Phased Array type L-band Synthetic Aperture Radar)

It is a Japan Aerospace Exploration Agency's ALOS mission (JAXA). The Advanced Land Observing Satellite-1 (ALOS), also known as DAICHI, carried three sensors, including PALSAR, that were designed to support mapping, precise regional land-cover observation, disaster monitoring, and resource surveys. The L-band synthetic aperture radar (SAR) of PALSAR provided comprehensive, all-weather, day-and-night observations as well as repeat-pass interferometry from 2006 to 2011. PALSAR data come from a variety of observational techniques with polarization, resolution, swath width, and off-nadir angle that are all varied, (https://asf.alaska.edu/data-sets/sar-data-sets/alos-palsar/alos-palsar-about/).

Table 2.2. ALOS Characteristics, after **(ibid).**

Launch Date	Jan. 24, 2006
Launch Vehicle	H-IIA
Launch Site	Tanegashima Space Center
Spacecraft Mass	Approx. 4 tons
Generated Power	3 -5 years
Design Life	3 -5 years
Orbit	Sun-Synchronous Sub-Recurrent
	Repeat Cycle: 46 days Sub Cycle: 2 days
	Altitude: 691.65 km (at Equator)
	Inclination: 98.16 deg.
Attitude Determination Accuracy	2.0×10^{-4}degree (with GCP)
Position Determination Accuracy	1m (off-line)
Data Rate	240Mbps (via Data Relay Technology Satellite) 120Mbps (Direct Transmission)
Onboard Data Recorder	Solid-state data recorder (90Gbytes)
Vertical accuracy	±25 m

Global vertical datum	North American Vertical Datum of 1988 (NAVD88) and Earth Gravitational Model of 1996 (EGM96)
Resolution	12.5 m
Generation technique	SAR interferometry
File format	Geo TIFF
Sensor type	Radar (L band)
Spatial extent	60^{o} N to 59^{o} S

2.5.2.1 Radiometric Terrain Correction applied to ALOS_PALSAR

The digital elevation model (DEM) file offered as part of ALOS_PALSAR terrain corrected product package is not created using PALSAR data directly. It is a duplicate of an existing DEM that has altered and then used to the radiometric terrain correction procedure. Although it is not a measure of the DEM’s resolution, the source DEM’s pixel spacing was altered to match that of the terrain corrected image it was included with.

The shuttle radar topography missions (SRTM) or the national elevation dataset (NED) provided the source DEM’s for the ALOS-PALSAR terrain corrected products (https://asf.alaska.edu/information/palsar-rtc-dem-information/).

Alaska Satellite Facilities (ASF's) Radiometric Terrain Correction Project: New ALOS-PALSAR RTC product releases started in October 2014 and ended a year later. Data from Fine Beam and Polarimetric sceneries are included in the RTC project, except for Antarctica, Greenland, Iceland, and northern Eurasia. ASF has developed products in 12.5 m and 30 m resolutions. The Alaska Satellite Facility's endeavor to provide radiometrically terrain corrected (RTC) products opens out SAR data to a larger consumer base. The project updates the data in the GIS-friendly GeoTIFF format and corrects the synthetic aperture radar (SAR) geometry and radiometry.

- The GeoTIFF-formatted DEM utilized for RTC processing:
- Pixel spacing is the same as the RTC GeoTIFF included in the package.
- Technical information is available in the RTC Product Guide and the ATBD (algorithm) information.
- Best resolution SRTM or NED source DEM currently available, with geoid correction applied.

Terrain Correction: Correcting geometric distortions that cause geolocation mistakes is known as terrain correction. Rugged terrain worsens the distortions, which are brought on by side-looking imagery rather than nadir imaging. Image pixels are moved by terrain correction into the correct spatial relationship with one another. Geolocation and shape correction is applied to mountains that appear to have tipped over in the direction of the sensor. When processing optical imagery, the correction of geometric distortion is frequently referred to as orthorectification.

Radiometric Terrain Correction: For science purposes, radiometric terrain correction combines the two corrections to provide a superior outcome. For biomass estimation, biodiversity evaluation, forest mapping, and monitoring, PALSAR and Landsat can be combined or used as complementing products.

Researchers now have a ready-made alternative to Landsat 8, an orthorectified product, in the form of ASF's RTC product.

PALSAR RTC DEM Information: Since most DEMs are geoid-based, they must be corrected before being applied to terrain correction. The DEM included with an ASF RTC product was transformed using the ASF Map Ready geoid adjust tool from the orthometric height of the source DEM to ellipsoid height. To ensure that the final DEM is related to the ellipsoid, this program applies a geoid adjustment (https://asf.alaska.edu/data-sets/sar-data-sets/alos-palsar/alos-palsar-about/)

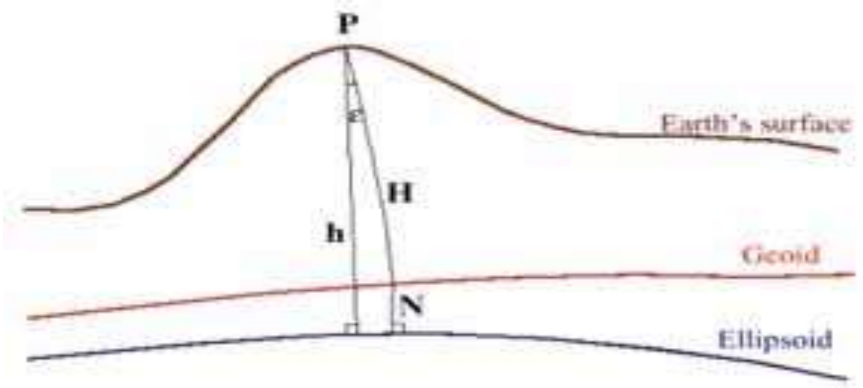

Figure 2.11. Orthometric and ellipsoidal heights relation through geoid undulations.

The quality of the digital elevation model (DEM) used in the radiometric terrain correction (RTC) procedure directly affects the quality of an ALOS-PALSAR RTC result.

The area covered by ALOS-PALSAR where one tile is 79 * 69 km.

CHAPTER THREE

INTERPOLATION AND ENHANCEMENT METHODS

CHAPTER 3: INTERPOLATION AND ENHANCEMENT METHODS

This chapter concerns the different related subjects to interpolation process. It defines the interpolation process and states the types of spatial interpolation and mentions the different interpolation techniques. The different methods of DEMs generation are explained. The role of interpolation methods in spatial enhancement of DEMs is described in addition to the DEMs accuracy assessment.

3.1 Definitions

Interpolation: is the process of computing an unknown value using provided values that are known, **(Wahab, 2017)**.

Spatial interpolation is the technique of estimating values at other sites using points with known values, **(Chang, 2008)**.

The spatial patterns collected by these measures can be compared with the spatial patterns of other spatial entities by interpolating data from point observations into continuous fields.

Spatial interpolation: is the process of estimating the value of attributes at unsampled places within the scope of the current observations, **(Setiyoko, 2013)**. As the number of known values increases, the predictions' accuracy significantly improves, **(Al-Mutairi et al., 2019)**.

The numbers and distribution of control points can have a significant impact on how accurately spatial interpolation is performed.

In GIS applications, a raster is often subjected to spatial interpolation, with estimations being made for each cell. Therefore, surface data can be produced from sample locations via spatial interpolation.

The spatial interpolation algorithms determine how accurate the resulting DEM will be. Many areas, including economics, business, population research, pricing determination, etc., use interpolation techniques. For the sake of information
continuity, it is employed to fill in the gaps in statistical data,
(https://csm.fresnostate.edu/ees/documents/facstaff/wang/gis200/lecture-notes/gis/chap15.pdf).

3.2 The Different Interpolation Concepts

The various interpolation methods include the spline method, cubic spline, shape-preserving cubic spline, radial basis functions, natural neighbor method, inverse distance weighting (IDW) method, and kriging interpolation method.

A function p(x) from a specified class of functions is chosen using the interpolation principle so that the graph of

$$y = p(x) \tag{3.1}$$

travels through a limited collection of available data points. The smoothing or interpolating function is denoted by the function p(x).

If p(x) is a polynomial, then the operation is known as polynomial interpolation and p(x) is referred to as the interpolating polynomial. Similar to this, trigonometric interpolation is available if p(x) is a finite trigonometric series. Interpolation theory is based on the calculus of finite differences, (Newton's Interpolation Methods (nitk.ac.in)).

There are several significant applications for polynomial interpolation theory. Its main functions are to provide certain mathematical tools for developing techniques in approximation theory, numerical integration, and the numerical solution of differential equations, (ibid).

3.3 DEM Generation Methods

Methods of DEM production:

3.3.1 Inverse Distance Weighting (IDW) Method

A precise method known as inverse distance weighted (IDW) interpolation ensures that close known points have a greater influence on a point's projected value than do points farther away.

The IDW method anticipates that the value at a remote site is frequently estimated as a weighted mean of the values at points within a particular cut-off distance or using collected data from numerous of the nearest places. This method essentially involves measuring the height of an unknown point by calculating its distance from other points that are known. IDW is an approach that is simple to use and convenient to access; it does not produce the implicit local shape through information and instead generates local highs at the points, **(Mitas and Mitasova, 2005)**.

A category of the multivariate mixed inverse distance weighting surfaces and volumes has offered some modification to move up, **(Watson, 1992)**.

The inverse distance weighting method's underlying premise is that measured points that are closer to an unknown point can have greater values than those that are farther away, **(Ikechukwu et al., 2017)**.

The power parameter's value has a significant impact on the precision of inverse distance weighting. Local spatial interpolation results from the weights decreasing with increasing distance, especially when the power parameter value increases. As a result, surrounding samples are given a higher weight and have a significant impact on estimate **(Isaaks and Srivastava, 1989)**. Power parameter and neighborhood size are random variables, **(Webster and Oliver, 2001)**. The most popular choice of p (is the power parameter that characterizes the rate of decrease of the weight as the distance gets bigger) is 2, and the method used to calculate the consequences is commonly known as inverse square distance or Inverse Distance Squared (IDS). The power parameter may also be chosen in accordance with the error measuring (such as the smallest absolute error), resulting in the best inverse distance weighting, **(Collins and Bolstad, 1996)**. The predicted results are found to be less good when p is one and two compared to when p is four because the softness for the predetermined surface differs directly with a power parameter, **(Ripley et al., 1981)**. When p is zero, inverse distance weighting is denoted as "moving average, **(Brus et al., 1996)**, when p is 1, "linear interpolation," and when p is not 1, "weighted moving average", **(Burrough, and McDonnell, 1998)**. Making "bull's-eyes" about where observations are located inside the gridded zone is one of IDW's strengths. The interpolated grid is smoothed using the smoothing parameter, reducing the "bull's-eye”effect.

$$Z(X,Y) = \frac{\sum_{i=1}^{n}\left[\frac{z_i}{d_i^p}\right]}{\sum_{i=1}^{n}\left[\frac{1}{d_i^p}\right]} \tag{3.2}$$

$$Z(X,Y) = \sum \lambda_{i\bullet} Z_i \xrightarrow{with} \sum \lambda_i = 1 \tag{3.3}$$

di: is the interpolation point's planimetric distance from the reference point, **(Robinson and Metternicht, 2006)**.

$$d_i = \sqrt{(X_i - X)^2 + (Y_i - Y)^2} \tag{3.4}$$

(x): is the expected value at the x, y point that was not sampled.

n: indicates the number of sample points that were measured and were local to the x, y area.

Zi: depicts the value that was observed at the i^{th} position.

λ: are the weights connected to each sample point that depend on distance.

di: is the distance between the measured location I and the predicted locations x, y.

p: is the power parameter that describes the rate at which the weight decreases as the distance increases.

n = 1, 2, 3,4,5……………...

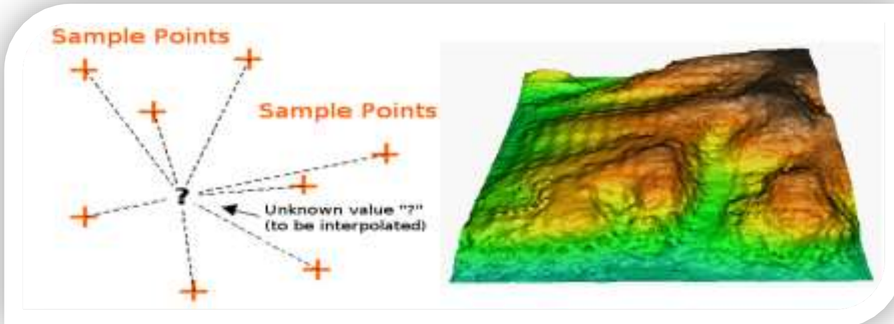

Figure 3.1. Inverse Distance Weighted (IDW), after **(https://gisresources.com/types-interpolation-methods_3)**

3.3.2 Kriging Interpolation Method

Kriging is a widely used and effective geostatistical gridding technique. With this technique, models from data with irregular spacing can be created. If you want an accurate grid of data, you can use the kriging defaults, or you can provide the right variogram model to make kriging specifically fit the data set, **(Zhu et al, 2013)**.

The weights of Ordinary Kriging are derived from the kriging equations using a semi-variance function. Semi-variograms are commonly represented by plotting the difference squared between the values of each pair of locations on the y-axis relative to the distance separating each pair on the x-axis.

$$\gamma h = \frac{1}{2N(h)} \sum_{i}^{N(h)} [Z(xi) - Z(xi+h)]^2 \qquad (3.5)$$

where Z(xi) and Z(xi+ h) are variable values on the xi, and xi+h points, respectively, and N(h) is the number of paired sample points separated by distance h.

- Geostatistical spatial interpolation is done using the kriging technique.
- Kriging uses estimated prediction errors to evaluate the accuracy of predictions.
- Kriging assumes that an attribute's spatial change is neither completely random (stochastic) nor predictable. Instead, the geographical variation might be composed of three elements: a random error term, a spatially correlated component that represents the variation of the regionalized variable, and a drift or structure that
  represents a trend,
  (https://csm.fresnostate.edu/ees/documents/facstaff/wang/gis200/lecture-notes/gis/chap15.pdf).

Different kriging techniques for spatial interpolation have been developed as a result of how these components are interpreted.

Kriging was founded on the concept of irregular functions with surface or volume indicated single attention for the random function with an accepted spatial covariance, **(Mitas, and Mitasova, 2005)**. This technique can be used for the derivation and plotting of point data while also providing a description of the semi-variance differences between neighboring values, **(Hengl, 2009)**. The following four sections can be used to exemplify the regionalized variable theory, which accepts the spatial variation surrounding each variable:

1) Consistent averages or patterns are a structural component.

2) A random component with a spatial connection that is a regionalized variable.

3) However, a random noise or residual component that is not tied to space.

4) Mathematically, the following compensation can be made for a random variable z at x:

$$Z(x) = m(X) + \varepsilon'(X) + \varepsilon'' \quad (3.6)$$

Where:

m(X): a structural function simulating an element of a structure,

ε'(X): the stochastic residual from m(X) that is spatially auto associated (the regionalized variable), ε'': Random noise that typically has a variation of σ^2 and an average of zero, **(Burrough and McDonnell, 1998)**.

There are three types of Kriging interpolation techniques: Regular Kriging, Basic Kriging, and Universal Kriging.

3.3.3 Natural Neighbor Method

The fundamental formula underlying the natural neighbor approach is, **(Boissonnat and Cazals, 2002):**

$$f(x) = \sum_{i=1}^{k} w_i(x)\, a_i \quad (3.7)$$

Where:

f(x) is an interpolated function valued at location x and ai (scalar value) is the attribute of each data point. The significance of the local coordinates affects the weights used in the natural neighbor interpolation approach. Any scatter point can own estimated value at the interpolation point if its local coordinates are considered to be "neighbourly" or a measure of effect. This closeness is entirely dependent on the area of the Thiessen polygons' influence on the surrounding scatter points, **(Ledoux and Gold, 2005)**.

The region of each Thiessen polygon in the network must be determined in order to obtain the local coordinates for interpolating the point Pn. Putting Pn into the Triangulated Irregular Network (TIN) tentatively causes the TIN and the associated Thiessen network to change, creating new Thiessen regions for polygons nearby Pn, **(Mohammed, 2004)**. Each neighbor is given consideration, and their weight is inversely proportionate to how far away they are from the interpolation position x. These concerns do not affect natural neighbor interpolation because the neighbors are chosen based on the information's creation, (ibid). The weights used in this interpolation method algorithm are proportionate to the "borrowed area," and they use the weighted mean of the nearby observations. The outline of the Thiessen polygons, for example, is no longer need to be anticipated by the Natural Neighbor approach behind the convex hull of the information positions, **(Yang, et al., 2004)**.

3.3.4 Spline Method

Thin-Plate Splines: A surface with the least amount of slope variation at every point is produced by thin-plate splines and passes through the control points. In other words, thin-plate splines have a minimum curvature surface and fit the control points.

These models relate the examined data points using mathematical operations. These models provide continuous elevation and grade surfaces while limiting the surface's generated curvature to the minimum,

(Ikechukwu, et al., 2017). The ability to build perfectly precise and aesthetically pleasing surfaces with only a small number of sample points is one of the spline's key advantages, **(Wu, et al., 2016)**. Spline functions are the mathematical analogues of the flexible ruler, or "spline," that cartographers used to fit wavy curves with numerous steady points. The spline is a piecewise polynomial with many parts, each of which rides on a small number of points, causing all of the sections to sign up at the break points. This is preferred over a simple polynomial interpolation because many parameters can be described, including the degree of smoothing, and has the advantage of absorbing local alterations, if there are variances about information in the spot. Small order polynomials (i.e., second or third order) that must sign up are typically used to fit the spline. When smoothing a contour line, for example, a spline may be either 2D or 3D. (in the modelling a surface). The smoothing spline function assumes that there is an estimating error in the data, which desires to be locally smoothed, **(Burrough and McDonnell, 1998)**. The thin-plate spline approach is the most widely used among the various variations and modulation of splines, additionally to the smoothing and pressure-regularized spline, **(Hutchinson, 1995)**.

3.4 Spatial Enhancement of DEMs

The vertical accuracy of remotely sensed DEMs varies depending on their source. LiDAR data, for instance, have a vertical accuracy of approximately 15 cm **(Carter, 2012)**. Many locations, especially in developing nations, lack access to reliable DEM sources like LiDAR. They only cover a small portion of space, and the data processing is complicated. To create DEMs with adequate accuracy and resolution, alternative techniques including spatial interpolation techniques must be used (i.e., kriging, Inverse distance weighting, Radial basis functions).

Whereas the vertical accuracy of DEMs from SRTM reaches ±16 m. When other values are available, spatial interpolation techniques are used to predict unknown values, such as elevations. The more known values there are, the more accurate the estimations become, **(Al-Mutairi et al., 2019)**. Deterministic or geostatistical techniques could be used for the spatial interpolation. Based on similarity or the degree of smoothing, deterministic interpolation methods such as inverse distance weighting (IDW) and radial basis function (RBF) generate surface grids from the measured points. The statistical characteristics of measured points are used by geostatistical techniques, such as kriging methods, to create surface maps, (ibid)

The following part illustrates some different methodologies applied by researchers to enhance the accuracy of DEMs.

1- Adding terrestrial GPS data and using the regression modelling method.

   The model is judged using the terrestrial GPS data and the statistics of height differences are calculated (average and standard deviation) as follow:

$$\Delta H_{i,j} = H_{i,j} - H_{DEM} \tag{3.8}$$

$$\bar{H}_i = \sum Hi \Big/ n \tag{3.9}$$

$$s_i = \sqrt{\sum (H_{i,j} - \bar{H}_i \Big/ n-1}$$ (3.10)

where,

$H_{i,j}$ is the known orthometric height of a control point no. j,

H_{DEM} is the corresponding orthometric height estimated from a specific DEM,

$\Delta H_{i,j}$ is the ith DEM error in estimating orthometric height for point j,

i range from 1 to 4 investigated models,

$\bar{H}_i$ represents the average height error for the i^{th} DEM,

s_i represents the standard deviation of height error for the i^{th} DEM,

Height errors over the control points will be spatially modeled by the regression analysis statistical toll which will be applied to model modelling differences (ΔH) as a function of Easting (Ei) and Northing (Ni) coordinates:

$$\Delta H_{i,j} = a_o + a_1 E_i + a_2 N_i$$ (3.11)

This equation will be written at a number of well distributed common points in the study area and they will be solved for the three unknown coefficients (a_o, a_1, and a_2).

The acquired coefficients will be applied to each station within the research area to produce the corresponding values of Δh, which will then be deducted from the model ellipsoidal heights to produce the corresponding model (estimated) ellipsoidal heights.

2- Using the kriging geostatistical method.

The change in the 3D surface is explained by taking into consideration the spatial distribution of the sample points.

$$\hat{Z}(S_o) = \sum_{i=1}^{n} \lambda_i Z(s_i) \qquad (3.12)$$

where,

$Z(s_i)$ is the measured quantity at the i^{th} location,

λ_i represents an unknown weight for point i,

s_o is the prediction location, and

n equals the measurements number.

The outcomes of the modelling phase will be evaluated over checkpoints.

3- Using the most recent and accurate local geoid model.

This method used to modify the accuracy of global digital elevation models by adopting recent and accurate global geoid model GGM which best fit to the study area.

$$H = h_{model} - N \qquad (3.13)$$

Where H is the orthometric height.

h is the ellipsoidal height.

N is the undulation of the recent and accurate geoid model.

Then get the difference between the model values and the estimated values as stated in equation (3.8). The statistics of the results (average and standard deviation) have been calculated as stated in equations (3.9) and (3.10).

4- Combining the model surface and the GPS ground control points utilizing the cubic convention resampling and the polynomial model.

a- 1st ,2nd or 3rd order polynomial can be used:

$$\begin{aligned} Z_{GPS} &= a_o + a_1E' + a_2N' + a_3Z' + \qquad \ldots(1^{st}\ \text{order}) \\ &+ a_4E'^2 + a_5N'^2 + a_6Z'^2 + a_7E'N' + a_8E'Z' + a_9N'Z' \qquad \ldots(2^{nd}\ \text{order}) \\ &+ a_{10}E'^3 + a_{11}E'^2N' + a_{12}E'N'^2 + a_{13}E'^2Z' + a_{14}E'Z'^2 \\ &+ a_{15}N'^3 + a_{16}N'^2Z' + a_{17}N'Z'^2 + a_{18}Z'^3 \qquad \ldots(3^{rd}\ \text{order}) \end{aligned} \tag{3.14}$$

Where:

Z_{GPS} is the elevation value of the GPS observed points,

N', E' and Z' are the corresponding SRTM DEM values of northing, easting, and elevation respectively,

a_0, a_1, a_2… the polynomial coefficients, **(Aguilar et al., 2007)**.

b- The model DEM is resampled using the cubic approach. This method of resampling DEM data is demonstrated in Figure (3.2), where the new cell value is determined by averaging the values of the 16 closest cells. The generated DTM will be smoothed and utilized for resampling continuous datasets, **(Grohmann, 2006)**.

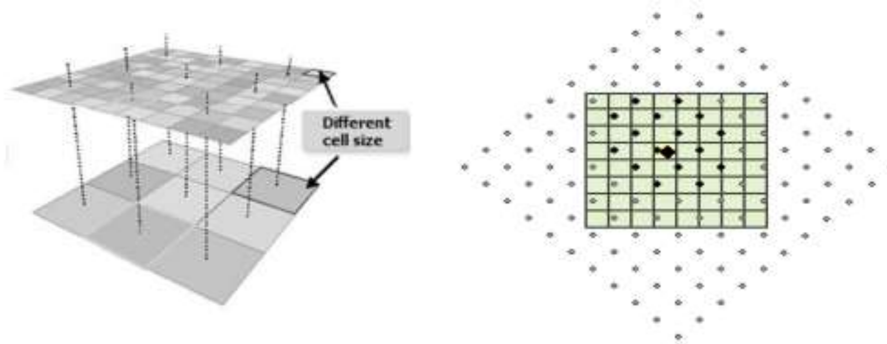

Figure 3.2. Cubic Convention Resampling, after **(El Sayed and Ali, 2016)**.

The polynomial will applied twice, one by using the original GDEM and the other by using the resampled GDEM by using cubic conventional resampling.

The polynomial coefficients will be generated using a set of common points and a software program for equation (3.14). The resulting coefficients and the SRTM coordinates of the check sites are then used to produce the interpolated coordinates. Then, along with their statistics, the height discrepancies between the interpolated coordinates and GPS of the check locations are determined for each research region.

In order to find the common and check points, the ground control points were observed using GPS technology.

Then get the difference between the model values and the estimated values as stated in equation (3.8). The statistics of the results (average and standard deviation) have been calculated as stated in equations (3.9) and (3.10).

3.5 Accuracy Assessment

Vertical accuracy, according to American Society for Photogrammetry and Remote Sensing (ASPRS) is the primary criterion in the specification of the quality of
elevation data,
(https://www.asprs.org/a/society/committees/lidar/Downloads/Vertical_Accuracy_Reporting_for_Lidar_Data.pdf). However, the vertical accuracy of a DEM is greatly influenced by its horizontal accuracy, which is also very important **(Sefercik and Ozendi, 2013)**. Absolute and relative vertical accuracy are the two forms of accuracy that can be identified when discussing a DEM's accuracy, **(Manune, 2007)**.

The vertical accuracy with respect to a Geodetic-Cartographic Reference System where an official altitude Datum has been accepted is known as the absolute vertical accuracy. The relative vertical accuracy, on the other hand, relates to the accuracy in relation to a local reference system. For the integration of altimetry data in frames relative to vast areas of interest, absolute precision is required. Only very local analyses are appropriate for relative accuracy, which is more closely tied to neighborhood-derived metrics (e.g., slope and aspect calculations), **(Seferick and Ozendi, 2013)**.

The accuracy of the elevation obtained at any point in a DEM is referred to as the vertical accuracy of the DEM. Its vertical accuracy is based on the differences between the elevations h_{DEM} evaluated in a particular location I and h_{REF} acquired from a source with greater accuracy in the same place I. Following **Florinsky (1998)**, we avoid using the term "error" here since it is insufficient given that the reference values utilized for the comparison are additionally impacted by their own uncertainty. In a similar manner, the

"Guide on the Expression of Uncertainty in Measurement" (https://www.iso.org/standard/50461.html) emphasizes that the "absolute error" is not regarded quantifiable or estimated, discouraging the use of this word since the real value cannot be known in any way. We can choose a value that is more closely related to the real value than another, but when all the variables that affect a measure's determination are taken into account, all values will always be subject to uncertainty, therefore the genuine value can never be known.

Yet anything that is more accurate than the one being examined will be treated as having actual worth. The statistical discrepancy between the true value and the observed value is what determines accuracy. In order to reduce the impact of the uncertainty of this value's h_{REF} on the accuracy estimation of h_{DEM}, the true actual value is roughly estimated by the source of greater accuracy (the reference).

Precision is a measure of dispersion, while truth is the absence of bias. This model works well for regularly distributed discrepancies where the bias is represented by the displacement parameter (μ) and the precision by the shape parameter (σ). **Butler (1998),** defined standards for DEM-related precision, reliability, and accuracy. Reliability is related to outliers in measurements or elaboration processes (e.g., ignoring the effects of lens distortion in photogrammetry); accuracy is related to systematic errors and precision is related to random errors of data sources (such as ground surveying, photogrammetry, lidar, etc.).

The values of the elevation discrepancies at each given point I, the mean of all these discrepancies, the standard deviation, and the root mean square error are given by the equations below **(ibid)**:

$$d_i = h_{DEM,\,i} - h_{REF,i}. \tag{3.15}$$

$$\mu_d = \frac{1}{n}\sum_{i=1}^{n} d_i \tag{3.16}$$

$$\sigma_d = \sqrt{\frac{1}{n-1}\sum_{i=1}^{n}(d_i - \mu)^2} \tag{3.17}$$

$$RMSE_d = \sqrt{\frac{1}{n}d_i^2} \tag{3.18}$$

Where:

$h_{DEM,i}$ elevation in position i of the DEM product

$h_{REF,i}$ elevation in position i of the reference

d_i discrepancy in elevation in position i and n number of samples

μ_d mean value of discrepancies

σ_d standard deviation of discrepancies

$RMSE_d$ root mean squared error of discrepancies

The interpolation methods applied to generate a high spatial resolution DEM were compared using cross validation. This was conducted by removing one data location and predicting the associated data using the data of the remaining locations. The accuracy of interpolation was done by calculating the deviations of interpolated elevation values from corresponding measured values in term of the Root Mean Square Error (RMSE):

$$RMSE = \sqrt{\frac{1}{n}\sum_{i=1}^{n}[z^{*}x_i - zx]^2} \tag{3.19}$$

Where zx is the observed value at location i, $z^{*}x_i$ is the interpolated value at location i, and n is the sample size.

Most researchers who have study DEMs and their applications proposed and used statistical measures, including the RMSE, to evaluate DEM reliability. Moreover, the correlation coefficient (R) was applied in order to examine the relationship between the predicted elevation points from the interpolated DEM and measured values taken from input spatial datasets. Higher values of (R) indicated higher significant correlations between datasets **(Al-Mutairi et al., 2019)**, where R is the proportion of the dependent variable's variance that the independent variable can account for. In other words, the coefficient of determination can be used to assess
how well the data fits the model (the goodness of fit),
(https://corporatefinanceinstitute.com/.../coefficient-of-determination).

In this thesis, DEMs are assessed by comparing their heights with the ground corresponding heights. Minimum, maximum, average, and standard deviations of the obtained differences are computed.

CHAPTER FOUR

DATA USED, METHODOLOGY, AND RESULTS

CHAPTER 4: DATA USED, METHODOLOGY, AND RESULTS

This chapter includes short description for the used data and the followed methodology to verify the goal of the research. The chapter also illustrates the obtained results and their analysis.

4.1 Data Used

Data used in this study contains: ground data, satellite data and geoid model data.

a- Ground data

- **Test Area 1**: A grid of 239 fixed points cover an area of 18.85 by 12.15 km in Toshka south of Egypt, about 55,000 Feddans, figure (4.1) and figure (4.2). The ellipsoidal coordinates of those points are obtained using GPS relative positioning. One of the High Accurate Reference Network (HARN) points is used as a reference station for the GPS work. Dual frequency receivers are used. The orthometric heights of those fixed points are obtained by traditional surveying methods related to the Egyptian Surveying Authority Benchmarks. The heights of test area 1 range from 234 to 280 m with average 248 m and standard deviation 17.5 m, figure (4.2).

- **Test Area 2**: a grid of 2722 points in the southwest of Egypt cover an area of 210 by 120 km, about 6 million Feddans, figure (4.1) and figure (4.3). GPS ellipsoidal heights of those points are available. Orthometric heights in this area are not available. Test area 2 is observed by Egyptian Surveying Authority (ESA). The heights of test

area 2 range from 347 to 707 m with average 476 m and standard deviation 81 m, figure (4.3).

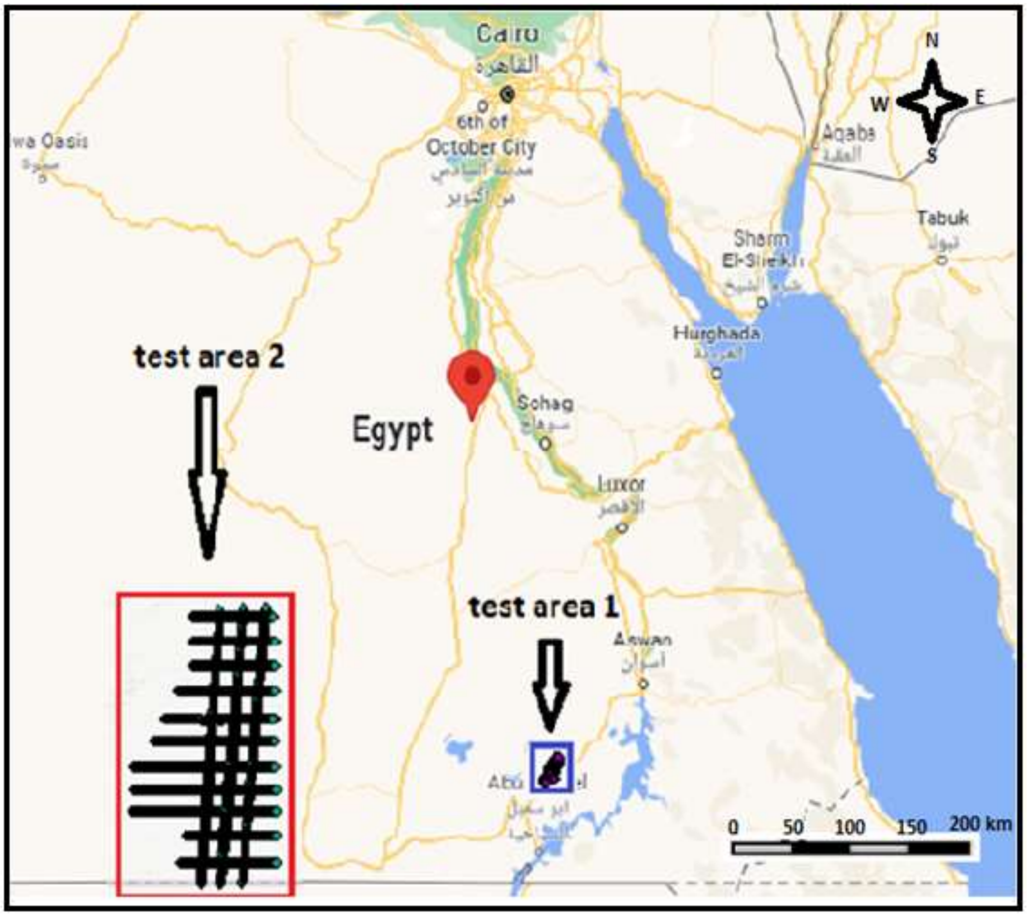

Figure 4.1. Test area 1, Toshka south of Egypt and Test area 2, southwest of Egypt.

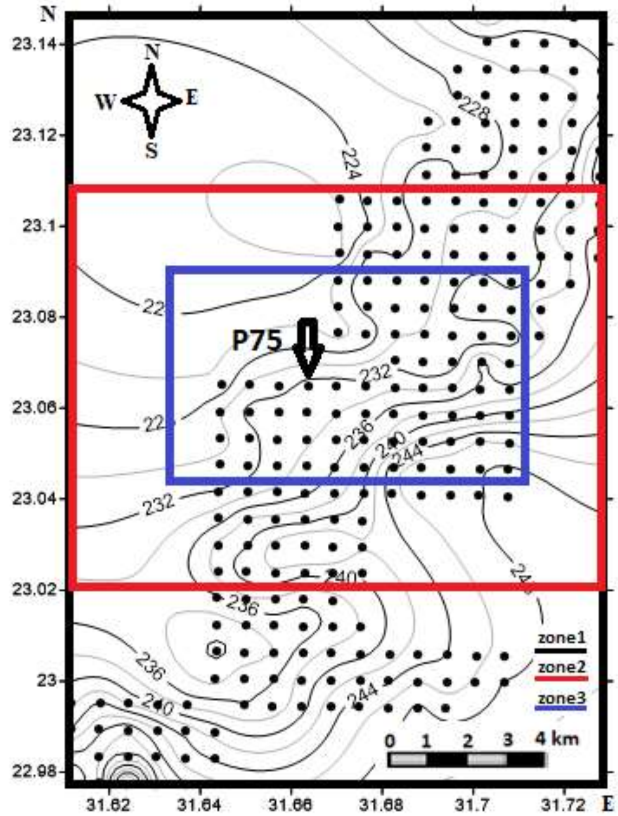

Figure 4.2. Study area 1 and its two subzones. 239, 139, and 81 points.

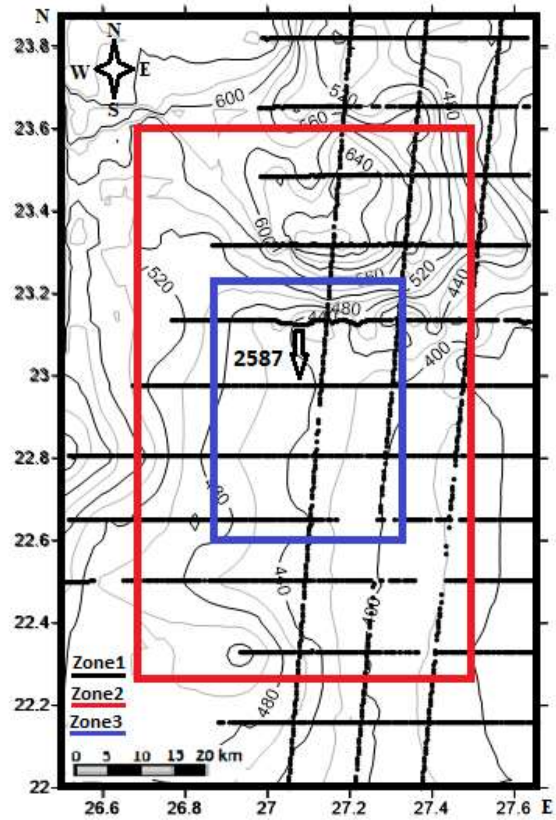

Figure 4.3. Test area 2 and its two subzones, 2722, 1532, and 534 points.

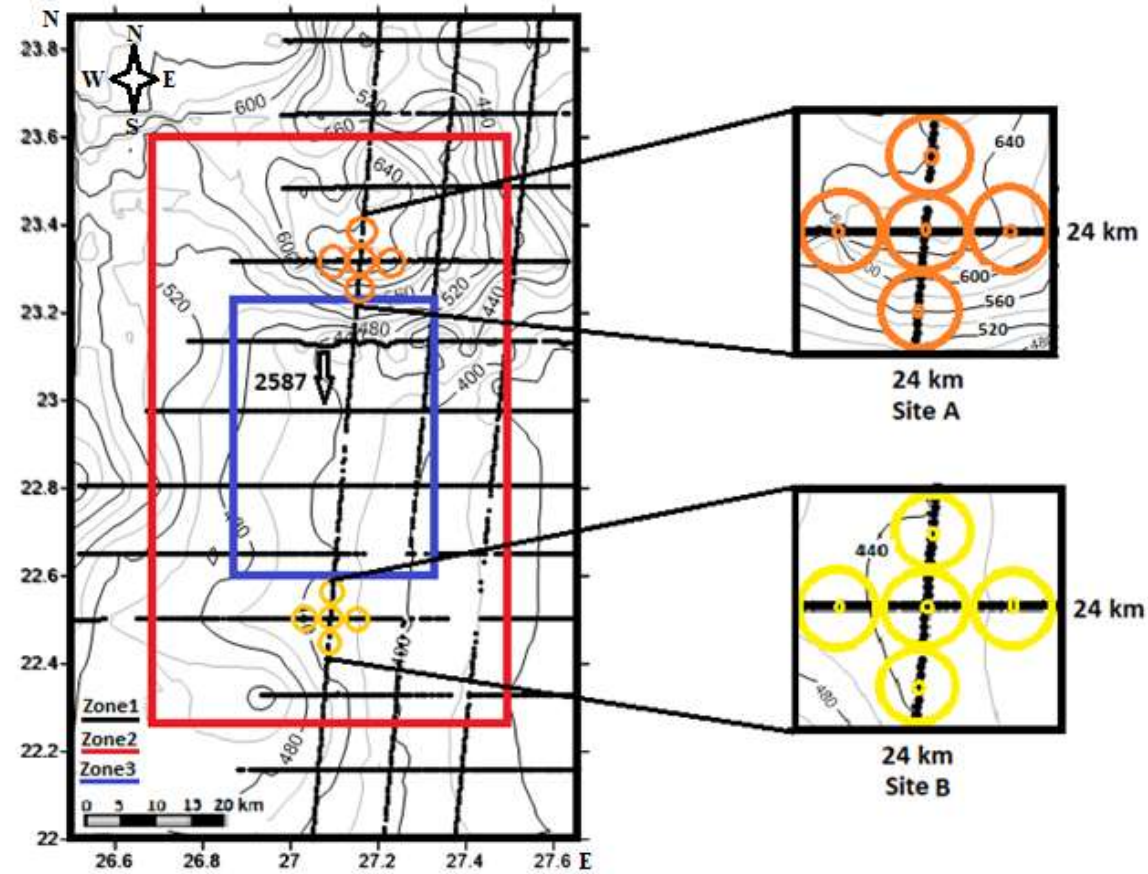

Figure 4.4. Test area 2, Site A, 76 points, 24 * 24 km, and Site B, 72 points, 24 * 24 km.

b- Satellite data

The shuttle radar topography mission (SRTM1) was selected in order to evaluate and enhance it in relation to the research area since, according to earlier studies, it is the most common and used of the other models. The ALOS-PALSAR was selected because it has a high resolution (12.5) m.

- **SRTM1 Global DEM** is produced in the year 2000 with 30 m resolution and ±16 m vertical precision,

  (https://www2.jpl.nasa.gov/srtm/). It is downloaded from Earth Explorer (https://earthexplorer.usgs.gov). All of the released products' original SRTM elevations were calculated according to the WGS84 ellipsoid, and then heights relative to the geoid were obtained by adding the EGM96 geoid separation values (https://en.wikipedia.org/wiki/Shuttle_Radar_Topography_Mission).

  The acquired elevations from SRTM1 are orthometric heights based on EGM96 geoid model.

- **ALOS_PALSAR Global DEM** is also used. It is produced in the year 2014 with 12.5 m resolution and produced different residual topography values of almost -20.5 m with a standard deviation of 33.24 m **(Darwish et al., 2021)**. Orthometric heights with the EGM96 vertical datum were provided by NASA. The ASF MapReady geoid adjust tool was used to convert them to ellipsoid heights, (https://asf.alaska.edu/information/palsar-rtc-dem-information/).

  The acquired elevations from ALOS_PALSAR are ellipsoidal heights.

c- Geoid model data

- The geoidal undulations from **(EGM96) and (SGG-UGM 2) global gravity models** are obtained from the official site of ICGEM, maximum used degrees are 360˚ for EGM96 and 2190˚ for **(SGG-UGM 2)**, reference system is WGS84 for the two geoid models. Resolution of the first is about 55 km and for the second is about 9 km. They are downloaded from ICGEM International Center for Global Gravity Field Models (gfz-potsdam.de).

4.2 Methodology

For both areas the following steps have been followed by first validating the data and then enhancing it as follows:

4.2.1 Evaluation process

Step a: Convert the ellipsoidal heights of ALOS-PALSAR to orthometric heights by using the geoid undulations of EGM96 as stated in equation (4.1) then Compares SRTM1 and ALOS-PALSAR orthometric heights with the corresponding field values based on EGM96. The differences and their statistics are computed by using equation (4.2)

$$H_{\text{ALOS-PALSAR}} = h_{\text{ALOS-PALSAR}} - N_{\text{EGM96}} \tag{4.1}$$

$$\Delta H_{\text{SRTM1 or ALOS-PALSAR}} = H_{\text{field}} - H_{\text{SRTM1 or ALOS-PALSAR}} \tag{4.2}$$

Where H_{field} is the orthometric height of the field data.

Step b: Converts the orthometric height of SRTM1 to ellipsoidal heights using the geoid undulations of EGM96 as stated in equation (4.3). Ellipsoidal heights of SRTM1 and ALOS-PALSAR are compared with their corresponding GPS field values. The differences are obtained, and their statistics are computed.

$$h_{SRTM1} = H_{SRTM1} + N_{EGM96} \qquad (4.3)$$

Where h is the ellipsoidal height

4.2.2 Improvement process

The improvement process is done using six different trials as follows:

- Shifting the orthometric heights of SRTM1 and ALOS-PALSAR by using one intermediate point.
- Shifting the ellipsoidal heights of SRTM1 and ALOS-PALSAR by using one intermediate point.
- Shifting once more but using five well-distributed points over the study area using equation (4.4).

The shifted model orthometric heights are compared with their corresponding field values, and the differences are computed, and their statistics also computed.

$$S = (H \text{ or } h)_{modified-} (H \text{ or } h)_{model} \qquad (4.4)$$

Where H_{model} is the orthometric height of model data, h_{model} is the ellipsoidal height of model data and S is the shift value.

- Least squares fitting polynomial is applied using the well-distributed five points as:

$$\Delta h = h_{field} - h_{model} = a_o + a_1 * \varphi + a_2 * \lambda \qquad (4.5)$$

Where:

- h_{model} is the ellipsoidal height obtained from the model.
- h_{field} is the ellipsoidal height obtained from GPS.
- φ, λ are the latitude and longitude of the point.

Solving equation (4.5) for well distributed five points in the study area, the three unknown coefficients (a_o, a_1, and a_2) can be obtained.

- Least squares fitting polynomial is applied using the well-distributed seven points as:

$$\Delta h = h_{field} - h_{model} = a_o + a_1 * \varphi + a_2 * \lambda + a_3 * \varphi * \lambda + a_4 * \varphi^2 + a5 * \lambda^2 \quad (4.6)$$

Solving equation (4.6) for well distributed seven points in the study area, the six unknown coefficients (a_o, a_1, a_2, a_3, a_4 and a_5) can be obtained.

The obtained coefficients will be applied to each station within the test area to obtain the corresponding Δh values. These differences will then be deducted from the model ellipsoidal heights to estimate the corresponding ellipsoidal heights, and the statistics of the differences will then be computed.

- Computes the orthometric height for ALOS-PALSAR and the new modified orthometric height for SRTM1 by subtracting the geoid undulations of SGG-UGM 2 from both global DEM's ellipsoidal heights as in equation (4.7).

$$H_{SRTM1\ or\ ALOS\_PALSAR} = h_{SRTM1\ or\ ALOS\text{-}PALSAR} - N_{SGG\text{-}UGM\text{-}2} \quad (4.7)$$

The orthometric height for ALOS-PALSAR and the new modified orthometric height for SRTM1 are tested against their corresponding field values, the differences are computed, and their statistics are illustrated.

4.3 Results and Analysis

4.3.1 Evaluation of SRTM1 and ALOS-PALSAR in Test area 1

The Evaluation process will be made over the whole area and two included smaller subzones, figure 4.2.

4.3.1.1 Testing SRTM1 and ALOS-PALSAR orthometric heights against field orthometric heights.

SRTM1 and ALOS-PALSAR orthometric heights are tested against field orthometric heights over the whole area and two included smaller subzones, figure (4.2). Both models based on EGM96. The statistics of the differences were calculated; see figures 4.5, 4.6, 4.7 and table 4.1.

In the three zones of different dimensions, the range and standard deviation of ALOS-PALSAR are bigger than their corresponding values of SRTM, but the average of ALOS-PALSAR is smaller than the average of SRTM. SRTM is more precise than ALOS-PALSAR, standard deviations of the first are smaller than those of the second.

4.3.1.2 Testing SRTM1 and ALOS-PALSAR ellipsoidal heights against GPS ellipsoidal heights, Test area 1

SRTM1 ellipsoidal heights are obtained by adding the geoidal undulations of EGM96 to SRTM1 orthometric heights. The SRTM1 and ALOS-PALSAR ellipsoidal heights are compared with their corresponding observed GPS values and the statistics of the differences were calculated; see figures 4.8, 4.9, 4.10 and table 4.2.

In the three zones and for both models, the range values are getting smaller when the test area gets smaller too. The average values of ALOS-PALSAR are less than those of SRTM1. The standard deviation values for every model slightly change with changing the dimensions. The standard deviations of SRTM1 are slightly better than those of ALOS-PALSAR.

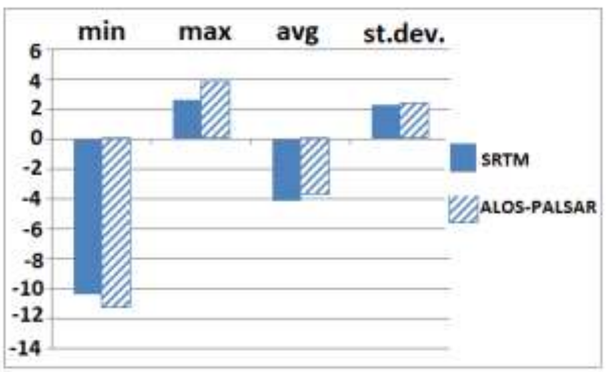

Figure 4.5. Zone 1, 239 points: $\Delta H_{field,SRTM1\ EGM96}$ and $\Delta H_{field,\ ALOS\text{-}PALSAR\ EGM96}$, 19 * 12 km, units in meters.

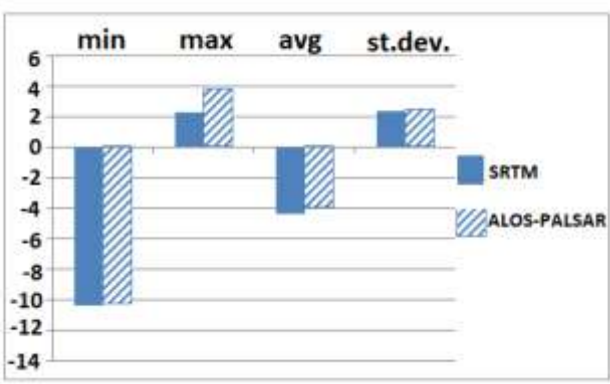

Figure 4.6. Zone 2, 138 points: $\Delta H_{field,SRTM1\ EGM96}$ and $\Delta H_{field,\ ALOS\text{-}PALSAR}$

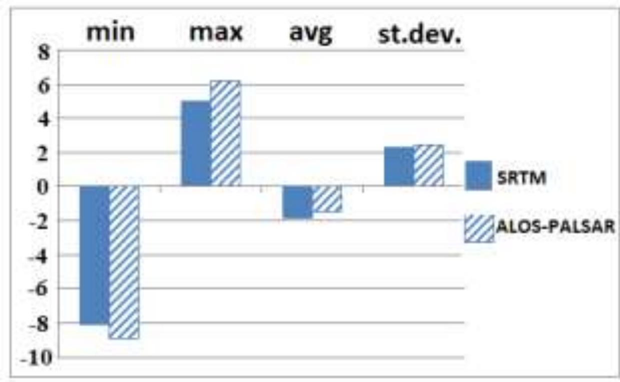

Figure 4.8. Zone 1, 239 points: $\Delta h_{field,\ SRTM1}$ and $\Delta h_{field,\ ALOS\text{-}PALSAR}$, 19 * 12 km, units in meters.

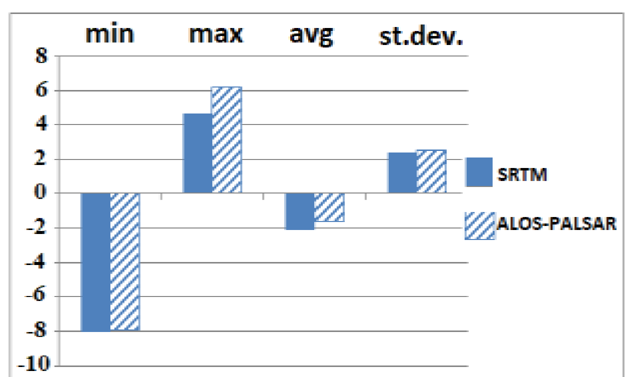

Figure 4.9. Zone 2, 138 points: $\Delta h_{field,\ SRTM1}$ and $\Delta h_{field,\ ALOS\text{-}PALSAR,}$ 12 * 9 km,

$_{EGM96}$, 12 * 9 km, units in meters.

units in meters.

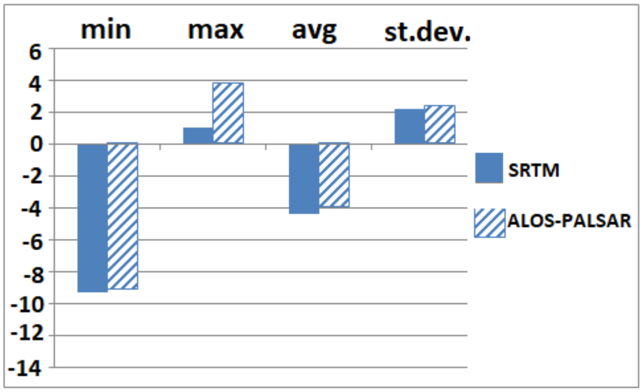

Figure 4.7. Zone 3, 81 points: $\Delta H_{field,SRTM1\ EGM96}$ and $\Delta H_{field,\ ALOS\text{-}PALSAR\ EGM96}$, 6.5 * 5 km, units in meters.

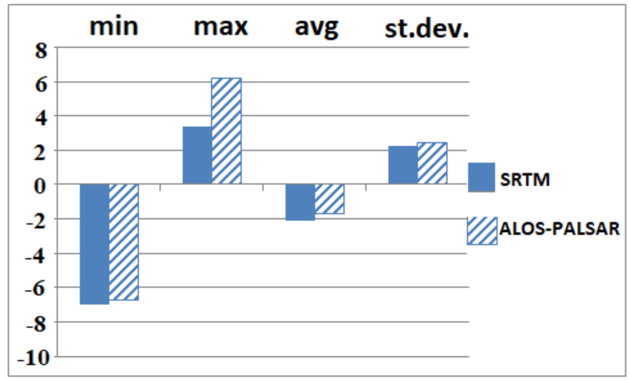

Figure 4.10. Zone 3, 81 points: $\Delta h_{field,\ SRTM1}$ and $\Delta h_{field,\ ALOS\text{-}PALSAR}$, 6.5 * 5 km, units in meters.

Table 4.1. Test area 1, Zone 1, Zone 2, and Zone 3, 239, 138, and 81 points respectively: $\Delta H_{field,SRTM1\ EGM96}$ and $\Delta H_{field,\ ALOS\text{-}PALSAR\ EGM96}$, units in meters.

	SRTM1			**ALOS-PALSAR**		
	Zone 1	Zone 2	Zone 3	Zone 1	Zone 2	Zone 3
Min	-10.38	-10.38	-9.28	-11.28	-10.32	-9.13
Max	2.63	2.27	1.04	3.79	3.79	3.79
Avg	-4.15	-4.37	-4.38	-3.76	-3.95	-3.97
st.dev.	2.27	2.38	2.23	2.38	2.5	2.4

Table 4.2. Test area 1, Zone 1, Zone 2, and Zone 3, 239, 138, and 81 points respectively: $\Delta h_{field,\ SRTM1}$ and $\Delta h_{field,\ ALOS\text{-}PALSAR}$, units in meters.

	SRTM1			**ALOS-PALSAR**		
	Zone 1	Zone 2	Zone 3	Zone 1	Zone 2	Zone 3
Min	-8.04	-8.04	-7.01	-8.93	-7.97	-6.76
Max	5	4.62	3.36	6.16	6.16	6.16

Avg	-1.87	-2.09	-2.09	-1.47	-1.67	-1.69
st.dev.	2.26	2.37	2.24	2.38	2.49	2.41

Excluding the geoid undulations, of EGM96, improved the averages from -4.15, -4.37, -4.37 m as orthometric case to -1.87, -2.09, -2.09 m in SRTM1 case. It also improved the averages from -3.75, -3.95, -3.97 m to -1.47, -1.67, -1.68 m with ALOS-PALSAR.

So, using ellipsoidal heights of DEMs is more reliable than using their orthometric heights. Then a trustable geoid model can be used.

4.3.2 Evaluation of SRTM1 and ALOS-PALSAR in Test area 2

The Evaluation process will be made over the whole area and two included smaller subzones, figure 4.3.

4.3.2.1 Testing SRTM1 and ALOS-PALSAR ellipsoidal heights against GPS ellipsoidal heights of Test area 2

SRTM1 and ALOS-PALSAR ellipsoidal heights are compared with their corresponding observed GPS values and the statistics of the differences were calculated:

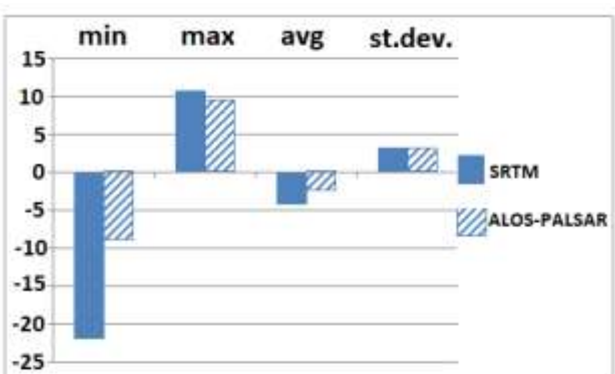

Figure 4.11. Zone 1, 2722 points $\Delta h_{field, SRTM1}$ and $\Delta h_{field, ALOS-PALSAR}$, 210 * 120 km,

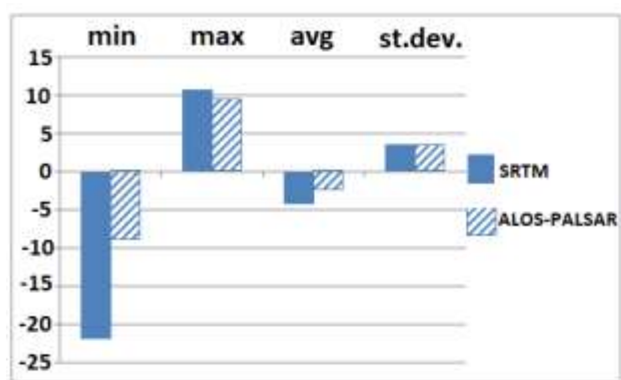

Figure 4.12. Zone 2, 1532 points: $\Delta h_{field, SRTM1}$ and $\Delta h_{field, ALOS-PALSAR}$, 143 * 81 km,

Test area 2, units in meters. Test area 2, units in meters.

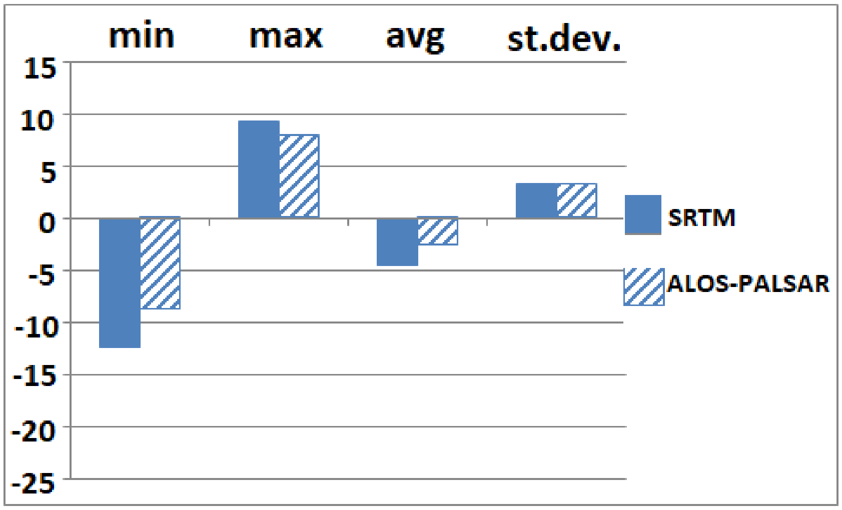

Figure 4.13. Zone 3, 534 points: Δh $_{\text{field, SRTM1}}$ and Δh $_{\text{field, ALOS-PALSAR}}$, 68 * 49 km, Test area 2, units in meters.

Table 4.3. Test area 2, Zone 1, Zone 2, and Zone 3, 2722, 1532, and 534 points respectively: Δh $_{\text{field, SRTM1}}$ and Δh $_{\text{field, ALOS-PALSAR}}$, units in meters.

	SRTM1			ALOS-PALSAR		
	Zone 1	Zone 2	Zone 3	Zone 1	Zone 2	Zone 3
min	-21.84	-21.84	-12.29	-8.97	-8.97	-8.80
max	10.66	10.66	9.39	9.45	9.45	7.99
Avg	-4.17	-4.28	-4.57	-2.40	-2.43	-2.64
st.dev.	3.17	3.54	3.28	3.14	3.38	3.26

In all three cases, range values of SRTM1 are bigger than those of ALOS-PALSAR and they generally are getting smaller as the test area getting smaller. The average values of ALOS-PALSAR are much smaller than those of SRTM1. Standard deviations of both models are close to each other's.

Comparing with the similar case in Test area 1, the range in Test area 2 is much bigger than that of Test area 1 when using SRTM1 and it is not far from its value in Test area 1 when using ALOS-PALSAR. In both models, the average and standard deviation values are much bigger in Test area 2 than those of Test area 1. The precision of the two models in Test area 2 are close to each other unlike the case of Test area 1. Recalling that Test area 2 is much bigger than Test area 1.

4.3.3 Improving the performance of SRTM1 and ALOS-PALSAR in Test area 1

4.3.3.1 Shifting SRTM and ALOS_PALSAR orthometric heights using one point

All points were shifted by a value of -4.12 m to SRTM and -3.95 m to ALOS-PALSAR, which corresponds to the differences between intermediate point's observed orthometric height and the corresponding model one over the whole area and two included smaller subzones, figure 4.2. The statistics of the differences were calculated; see figures 4.14, 4.15, 4.16 and table 4.4.

In the three different areas, the range is getting smaller when the area is getting smaller too in both cases of SRTM1 and ALOS-PALSAR. The ranges of ALOS-PALSAR are always larger than those of SRTM1. The standard deviations of ALOS-PALSAR are larger than those of SRTM1. Again, SRTM1 is more precise than ALOS-PALSAR.

Comparing the shift results with the orthometric heights without shift, the average values are less significantly after shift. They were -4.15, -4.37, -4.37 m before shift and they became -0.03, -0.25, -0.25 m after shift in case of

SRTM1. In case of ALOS-PALSAR, they were -3.75, -3.95, -3.97 m and became 0.19, 0.00, -0.02 m.

Shifting process doesn’t affect the standard deviations because the internal relation between the values stills the same.

4.3.3.2 Shifting SRTM1 and ALOS-PALSAR ellipsoidal heights using one point

All points were shifted by a value of -1.89 m to SRTM1 and -1.71 m to ALOS-PALSAR, which corresponds to the difference between intermediate point's GPS ellipsoidal height and its model ellipsoidal height over the whole area and two included smaller subzones, figure 4.2. The statistics of the differences were calculated; see figures 4.17, 4.18, 4.19 and table 4.5.

In the three different areas, the range is getting smaller when the area is getting smaller too in both cases of SRTM1 and ALOS-PALSAR. The ranges of ALOS-PALSAR are always larger than those of SRTM1. The standard deviations of ALOS- PALSAR are larger than those of SRTM1. Again, SRTM1 is more precise than ALOS-PALSAR.
Comparing the shift results with the ellipsoidal heights without shift, the average values are less significantly after shift. They were -1.87, -2.09, -2.09 m before shift and they became 0.02, -0.20, -0.20 m after shift in case of SRTM1. In case of ALOS- PALSAR, they were -1.47, -1.67, -1.69 m and became 0.24, 0.04, 0.02 m.

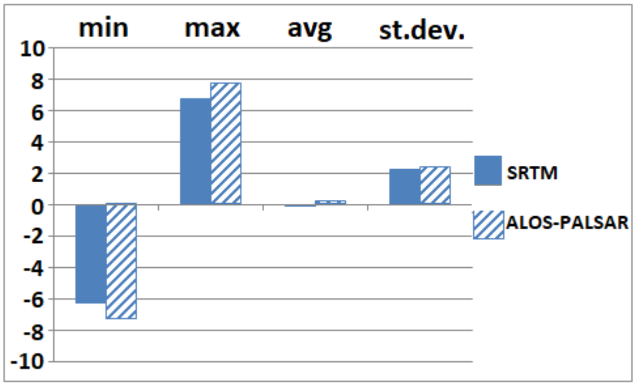

Figure 4.14. Zone 1, $\Delta H_{\text{field, SRTM1 EGM96}}$ and $\Delta H_{\text{field, shifted ALOS-PALSAR EGM96}}$.

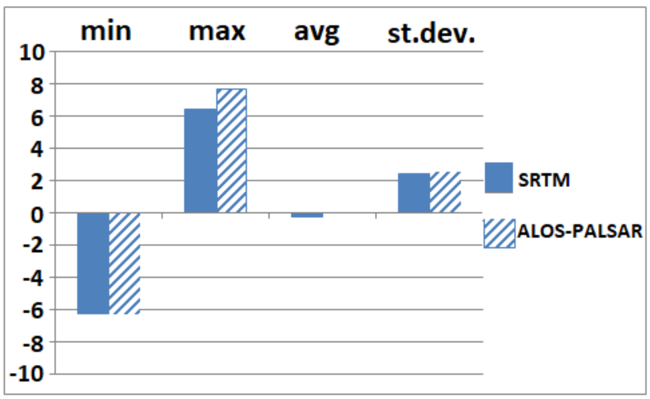

Figure 4.15. Zone 2, $\Delta H_{\text{field, SRTM1 EGM96}}$ and $\Delta H_{\text{field, shifted ALOS-PALSAR EGM96}}$.

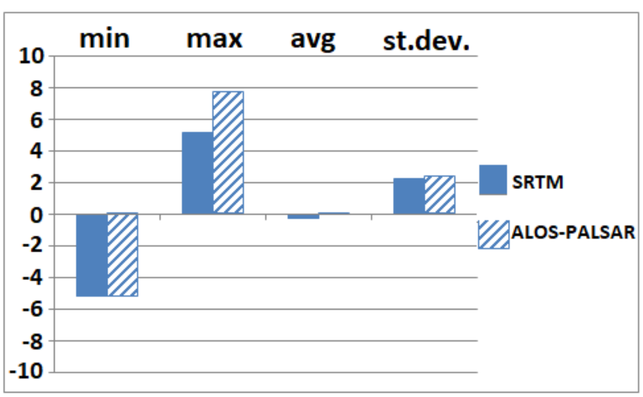

Figure 4.16. Zone 3, $\Delta H_{\text{field, SRTM1 EGM96}}$ and $\Delta H_{\text{field, shifted ALOS-PALSAR EGM96}}$.

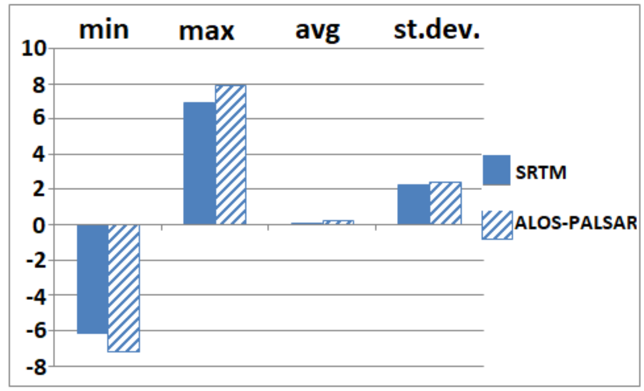

Figure 4.17. Zone 1, $\Delta h_{\text{field, SRTM1}}$ and $\Delta h_{\text{field, shifted ALOS-PALSAR}}$.

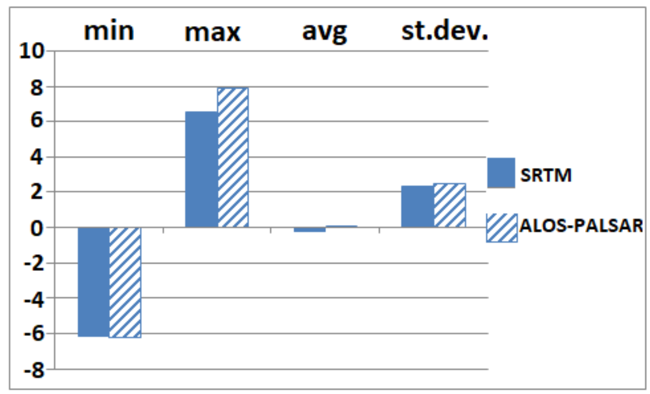

Figure 4.18. Zone 2, $\Delta h_{\text{field, SRTM1}}$ and $\Delta h_{\text{field, shifted ALOS-PALSAR}}$.

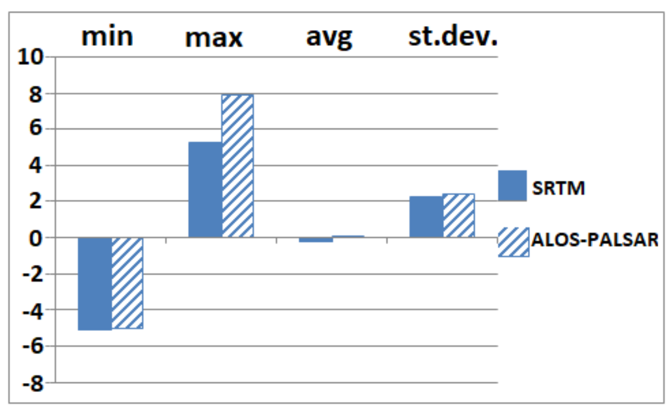

Figure 4.19. Zone 3, $\Delta h_{\text{field, SRTM1}}$ and $\Delta h_{\text{field, shifted ALOS-PALSAR}}$.

Table 4.4. Test area 1, Zone 1, Zone 2, and Zone 3, 239, 138, and 81 points respectively: $\Delta H_{\text{field, SRTM1 EGM96}}$ and $\Delta H_{\text{field, shifted ALOS-PALSAR EGM96}}$.

	SRTM1			ALOS-PALSAR		
	Zone 1	Zone 2	Zone 3	Zone 1	Zone 2	Zone 3
Min	-6.25	-6.25	-5.16	-7.33	-6.37	-5.18
Max	6.76	6.40	5.17	7.74	7.74	7.74
Avg	-0.03	-0.25	-0.25	0.19	-0.003	-0.02
st.dev.	2.27	2.36	2.23	2.38	2.49	2.40

Table 4.5. Test area 1, Zone 1, Zone 2, and Zone 3, 239, 138, and 81 points respectively: $\Delta h_{\text{field, SRTM1}}$ and $\Delta h_{\text{field, shifted ALOS-PALSAR}}$.

	SRTM1			ALOS-PALSAR		
	Zone 1	Zone 2	Zone 3	Zone 1	Zone 2	Zone 3
min	-6.15	-6.15	-5.13	-7.23	-6.26	-5.06
max	6.89	6.51	5.24	7.87	7.87	7.87
Avg	0.02	-0.20	-0.20	0.24	0.04	0.02
st.dev.	2.28	2.37	2.24	2.38	2.49	2.41

Shifting process doesn't affect the standard deviations because the internal relation between the values stills the same.

So, shifting process improves the average significantly and does not affect the precision of the model.

4.3.3.3 Improving the performance of SRTM1 and ALOS-PALSAR using 1st and 2nd order polynomials

Applying a 1st order and 2nd order polynomial in latitude and longitude at number of common points as stated in equations (4.5) and (4.6) respectively.

The two equations will be written at a number of well-distributed common points in the study area:

- They will be solved for the three unknown coefficients (a_o, a_1, and a_2) in a 1st-order polynomial using five points. The acquired coefficients a0, a1, a2 are -20.13, -0.56 and 1.04 respectively.
- They will be solved for six unknown coefficients (a_0, a_1, a_2, a_3, a_4, and a_5) in a 2nd-order polynomial using seven points. The acquired coefficients a0, a1, a2, a3, a4 and a5 are 13194.14, -37478.00, 26428.00, 1194.38, -8.26 and -851.26 respectively.

The acquired coefficients will be applied to each station within the research area to produce the corresponding values of Δh, which will then be deducted from the model ellipsoidal heights to produce the corresponding model (enhanced) ellipsoidal heights.

To evaluate the improvement process, statistics (max, min, avg, and st.dev.) will be performed for the differences between the estimated values and their corresponding field values.

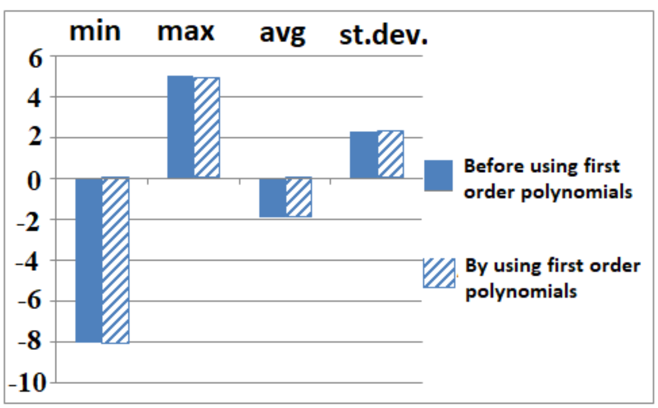

Figure 4.20. Zone 1, SRTM1 ellipsoidal heights, enhanced by using 1st order polynomials.

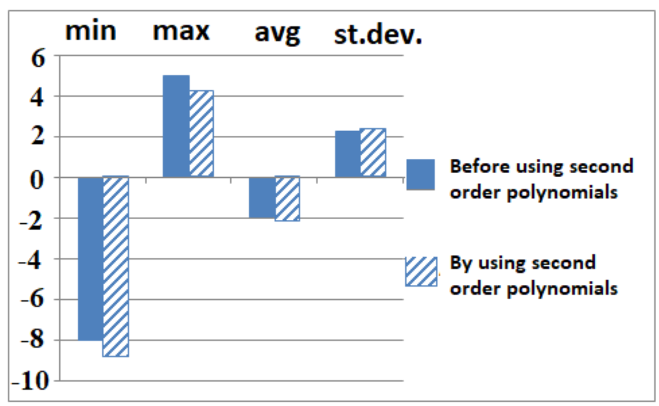

Figure 4.21. Zone 1, SRTM1 ellipsoidal heights, enhanced by using 2nd order polynomials.

The 2nd order polynomial did not improve the results compared to the 1st order one.

Table 4.6. Test area 1, Zone 1, SRTM1 ellipsoidal heights, enhanced by using 1st and 2nd order polynomials, units in meters.

	Before using polynomials	By using first order polynomials	By using second order polynomials
Min	-8.04	-8.11	-8.87
Max	5.00	4.92	4.24
Avg	-1.91	-1.96	-2.15
st.dev.	2.26	2.26	2.35

4.3.3.4 Improving SRTM1 and ALOS-PALSAR orthometric heights by replacing SGG-UGM2 instead of EGM96

The ellipsoidal heights of SRTM1 and ALOS-PALSAR are transformed into their corresponding orthometric heights by subtracting the undulation values of one of the recent Earth-Geoid-Models (SGG-UGM 2) over the whole area and two included smaller subzones, figure 4.2. The new obtained orthometric heights of SRTM1 and ALOS-PALSAR are then compared to the field orthometric heights.

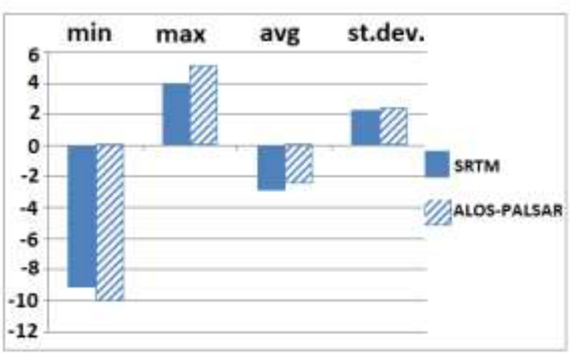

Figure 4.22. Zone 1, ΔH $_{\text{field}}$, $_{\text{SRTM1 SGG-UGM 2}}$ and ΔH $_{\text{field}}$, $_{\text{ALOS-PALSAR SGG-}}$

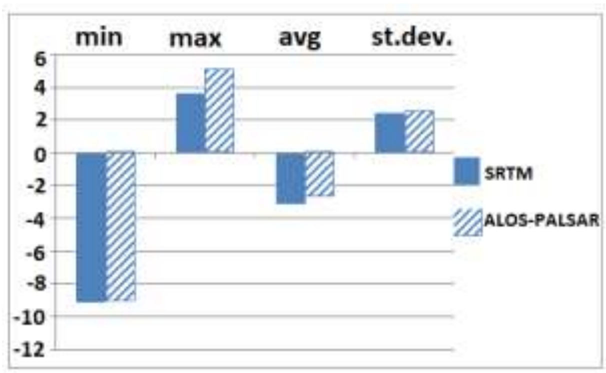

Figure 4.23. Zone 2, ΔH $_{\text{field}}$, $_{\text{SRTM1 SGG-UGM 2}}$

UGM 2·UGM 2· and ΔH $_{field}$, $_{ALOS\text{-}PALSAR\ SGG\text{-}UGM\ 2}$·

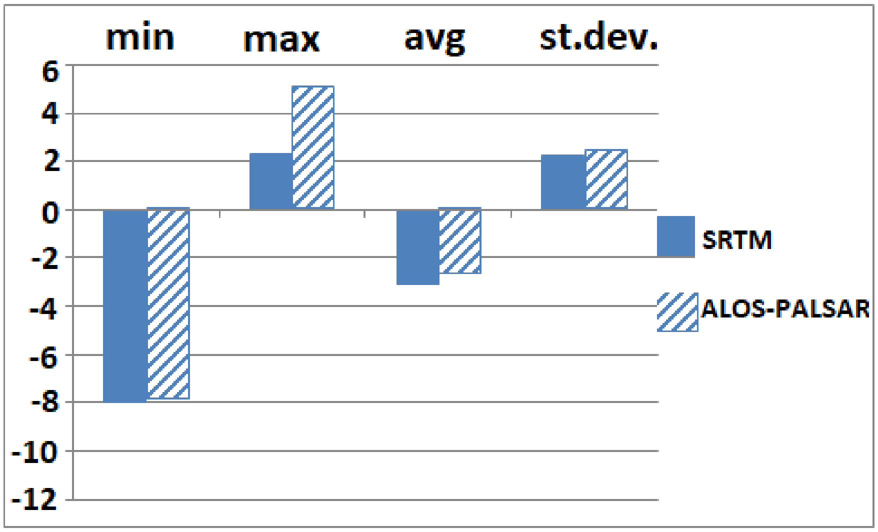

Figure 4.24. Zone 3, ΔH $_{field}$, $_{SRTM1\ SGG\text{-}UGM\ 2}$ and ΔH $_{field}$, $_{ALOS\text{-}PALSAR\ SGG\text{-}UGM\ 2}$·

Table 4.7. Test area 1, Zone 1, Zone 2, and Zone 3, 239, 138, and 81 points respectively: ΔH $_{field}$, $_{SRTM1\ SGG\text{-}UGM\ 2}$ and ΔH $_{field}$, $_{ALOS\text{-}PALSAR\ SGG\text{-}UGM\ 2}$, units in meters.

	SRTM1			**ALOS-PALSAR**		
	Zone 1	Zone 2	Zone 3	Zone 1	Zone 2	Zone 3
Min	-9.08	-9.08	-7.99	-10.00	-9.01	-7.82
Max	3.91	3.58	2.34	5.10	5.10	5.10
Avg	-2.87	-3.08	-3.08	-2.47	-2.66	-2.68
st.dev.	2.27	2.36	2.23	2.38	2.49	2.41

In the three areas and for both models, the range values decrease with decreasing the test area. For SRTM1, standard deviation values decrease with decreasing the test area. The average values of ALOS- PALSAR are smaller than those of SRTM1.

Standard deviation values of SRTM1 are smaller than those of ALOS-PALSAR. It means again that SRTM1 is more precise than ALOS-PALSAR.

Using SGG-UGG 2 instead of EGM96 changed the average values from -4.25, -4.37, -4.37 m to -2.87, -3.08, -3.08 m in case of SRTM1, while they changed from -3.75, -3.95, -3.97 m to -2.47, -2.65, -2.67 m in case of ALOS-PALSAR. The standard deviation values did not change due to changing the used geoid model.

Still using the ellipsoidal heights of a DEM is better than using its orthometric heights regarding the average values. Using ellipsoidal heights gave -1.87, -2.09, -2.09 m and using orthometric heights gave -2.87, -3.08, -3.08 m in case of SRTM1 while using ellipsoidal heights gave -1.47, -1.67, -1.68 m and using the orthometric heights gave -2.47, -2.65, -2.67 m in case of ALOS-PALSAR.

4.3.3.5 Shifting modified SRTM1 and ALOS-PALSAR orthometric heights using one point

All points were shifted by a value of -2.84 m to SRTM1 and -2.66 m to ALOS-PALSAR, which corresponds to the difference between an intermediate point's observed orthometric height and the corresponding modified model one over the whole area and two included smaller subzones, figure 4.2.

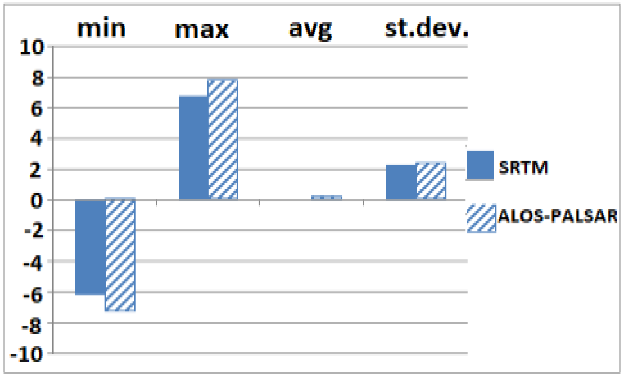

Figure 4.25. Zone 1, ΔH $_{\text{field, shifted SRTM1 SGG-UGM 2}}$ and ΔH $_{\text{field, shifted ALOS-PALSAR SGG-UGM 2}}$.

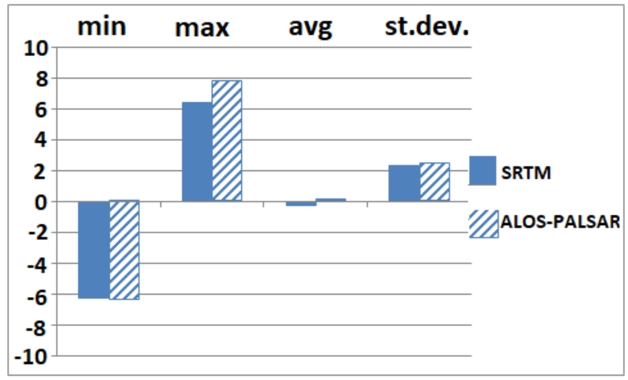

Figure 4.26. Zone 2, ΔH $_{\text{field, shifted SRTM1 SGG-UGM 2}}$ and ΔH $_{\text{field, shifted ALOS-PALSAR SGG-UGM 2}}$.

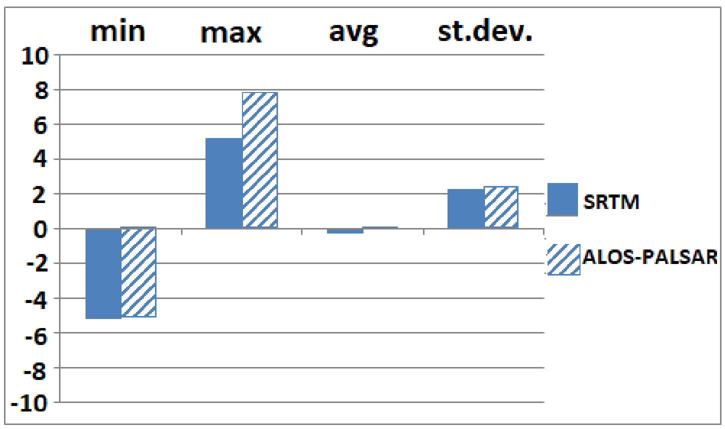

Figure 4.27. Zone 3, ΔH $_{\text{field, shifted SRTM1 SGG-UGM 2}}$ and ΔH $_{\text{field, shifted ALOS-PALSAR SGG-UGM 2}}$.

Table 4.8. Test area 1, Zone 1, Zone 2, and Zone 3, 239, 138, and 81 points respectively: ΔH $_{\text{field, shifted SRTM1 SGG-UGM 2}}$ and ΔH $_{\text{field, shifted ALOS-PALSAR SGG-UGM 2}}$, units in meters.

	SRTM1			ALOS-PALSAR		
	Zone 1	Zone 2	Zone 3	Zone 1	Zone 2	Zone 3
Min	-6.24	-6.24	-5.15	-7.34	-6.36	-5.16
Max	6.75	6.42	5.18	7.75	7.75	7.75
Avg	-0.03	-0.24	-0.24	0.17	0.002	-0.02
st.dev.	2.27	2.36	2.23	2.39	2.49	2.40

In the three areas, the range and standard deviation values of ALOS-PALSAR are larger than those of SRTM1. The average values are better (smaller) than those of SRTM1. For both DEMs the standard deviation values are getting smaller as the test area getting smaller too.

The same results are obtained in shifting modified orthometric (SGG-UGG 2) heights and shifting the orthometric heights (EGM96) and both cases are close to shifting the ellipsoidal heights.

4.3.4 Improving SRTM1 and ALOS-PALSAR in Test area 2

Test area 2 is large, 210 *120 km. It is useful to examine the proposed shifting process on such a large area. Both models will be improved once in three large areas approximately 210 *120 km, 143 *81 km, 68 *49 km and once more by taking two sample sites, one in flat terrain and the other one in moderate slope area.

4.3.4.1 Shifting ellipsoidal heights of SRTM1 and ALOS-PALSAR using one point

Ellipsoidal heights of SRTM1 and ALOS-PALSAR are shifted by a value of -3.961m to SRTM1 and -2.269 m to ALOS-PALSAR which corresponds to the difference between intermediate point's GPS ellipsoidal height and its model ellipsoidal height over the whole area and two included smaller subzones as shown in figure 4.3. The statistics of the differences between the field and model data were calculated; see figures 4.28, 4.29, 4.30 and table 4.9.

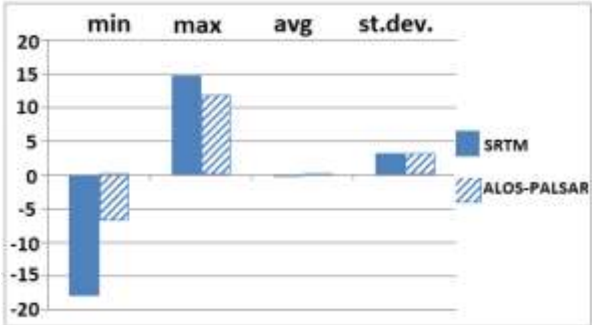

Figure 4.28. Zone 1, 2722 points: Δh $_{field, SRTM1}$ and Δh $_{field, shifted ALOS-PALSAR}$.

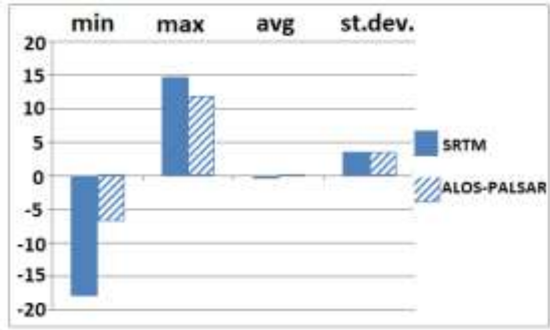

Figure 4.29. Zone 2, 1532 points, Δh $_{field, SRTM1}$ and Δh $_{field, shifted ALOS-PALSAR}$.

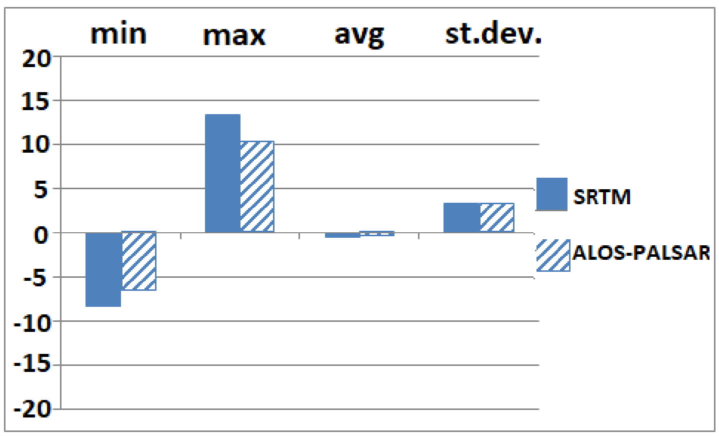

Figure 4.30. Zone 3, 534 points, Δh $_{field, SRTM1}$ and Δh $_{field, shifted ALOS-PALSAR}$.

Table 4.9. Test area 2, Zone 1, Zone 2, and Zone 3, 2722, 1532, and 534 points respectively: Δh $_{field, SRTM1}$ and Δh $_{field, shifted ALOS-PALSAR}$, units in meters.

	SRTM1			ALOS-PALSAR		
	Zone 1	Zone 2	Zone 3	Zone 1	Zone 2	Zone 3
Min	-17.88	-17.88	-8.33	-6.70	-6.70	-6.53
Max	14.62	14.62	13.35	11.72	11.72	10.26

Avg	-0.21	-0.31	-0.60	-0.13	-0.16	-0.37
st.dev.	3.17	3.54	3.28	3.14	3.38	3.26

In all three cases, range values of SRTM1 are bigger than those of ALOS-PALSAR and they generally are getting smaller as the test area gets smaller. The average values of ALOS-PALSAR are smaller than those of SRTM1. Standard deviations of both models are close to each other's. The shifting process reduced the average values from -4.17, -4.27, -4.56 to -0.21, -0.31, -0.60 m in the case of SRTM1 and reduced them from -2.40, -2.42, -2.64 to -0.13, -0.16, -0.37 m in the case of ALOS-PALSAR.

It should be noticed that those resulted values are for large areas with areas approximately 210 *120 km, 143 *81 km, 68 *49 km respectively and they are close to the results acquired by one point shift in test area 1. It should also be noticed that the average values decrease while the radius of the shifted area increases.

4.3.4.2 Improving SRTM1 and ALOS-PALSAR in two different topographic sites

Two sites, different in topography, are chosen for this test. One of them has low rough slopes (site A) and the other one is a flat area (site B) as shown in figure (4.4). Each of the two sites has an area 24 * 24 km.

In each of the two sites, five evenly distributed points were employed, each with a 4 km radius:

- The five points are used separately to shift the points that fell within their assigned ranges. Shifting values in site A are -5.12, -

7.42, -6.65, -6.02, -6.04 m and in site B are -4.34, -4.43, -0.97, -2.11 and -2.88 m.

- First and second-order polynomials are used in the enhancement process; five and seven points are used respectively.
    - For site A: They will be solved for the three unknown coefficients (a_o, a_1, and a_2) in a 1st-order polynomial using five points. The acquired coefficients a0, a1, a2 are 23.57, -10.69 and 8.08 respectively. They will be solved for six unknown coefficients (a_0, a_1, a_2, a_3, a_4, and a_5) in a 2nd-order polynomial using seven points. The acquired coefficients a0, a1, a2, a3, a4 and a5 are 29429715.81, -1172548.90, -1160515.19, 50590.72, -4320.62 and -351.57 respectively.
    - For site B: They will be solved for the three unknown coefficients (a_o, a_1, and a_2) in a 1st-order polynomial using five points. The acquired coefficients a0, a1, a2 are 801.10, -14.66 and -17.49 respectively. They will be solved for six unknown coefficients (a_0, a_1, a_2, a_3, a_4, and a_5) in a 2nd-order polynomial using seven points. The acquired coefficients a0, a1, a2, a3, a4 and a5 are -411669.84, 14742.71, 18153.69, -358.30, -112.11 and -186.23 respectively.

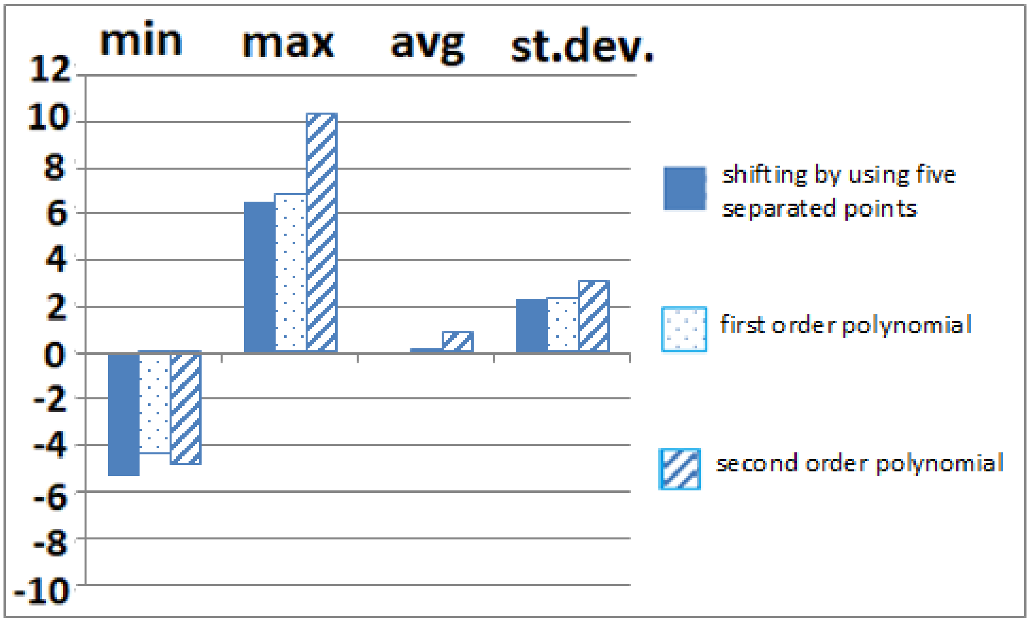

Figure 4.31. Site A, 76 points, shifting using five separated points, 1st and 2nd order polynomials, $\Delta h_{\text{field, model (modified)}}$.

Table 4.10. Site A, 76 points, shifting using five separated points, 1st and 2nd order polynomials, $\Delta h_{\text{field, model (modified)}}$, units in meters.

	five separated points	first order polynomials	second order polynomials
Min	-5.30	-4.42	-4.84
Max	6.50	6.80	10.29
Avg	-0.11	0.12	0.89
st.dev.	2.34	2.36	3.03

Figure 4.32. Site B, 72 points, shifting using five separated points, 1st and 2nd order polynomials, $\Delta h_{\text{field, model (modified)}}$.

Table 4.11. Site B, 72 points, shifting using five separated points, 1st and 2nd order polynomials, $\Delta h_{\text{field, model (modified)}}$, units in meters.

	using five separated points	**first order polynomial**	**second order polynomial**
Min	-8.51	-8.57	-6.93
Max	8.99	8.27	10.20
Avg	0.02	-0.14	1.73
st.dev.	3.95	3.95	4.22

In site A, shifting using 5 separated points, 1^{st} order polynomial and 2^{nd} order polynomial gave average values -0.11, 0.12 and 0.89 m respectively, while in site

B, they gave average values 0.02, -0.14 and 1.37 m respectively. The proposed shifting process has too small average relative to the other two polynomials.

In both sites, the standard deviation of shifting using five separated points and first order polynomials is smaller, while that of the second-order polynomials is large.

From the acquired results, the proposed shifting process is much more effective in flat and moderate slopes areas.

CHAPTER FIVE

SUMMARY, CONCLUSIONS AND RECOMMENDATIONS

CHAPTER 5: SUMMARY, CONCLUSIONS AND RECOMMENDATIONS

5.1 Summary

Representing the earth surface topography is necessary in many applications and uses; we will need long time and great efforts to do this by the ground techniques. The revolution of satellite mapping enabled obtaining digital elevation model to wide area of the earth surface. So, the presentation of the earth surface became easier and saves time and efforts. Unfortunately, the problem of this way is the low accuracy of these DEMs in many places according to the nature of the earth surface and the absence of the data in other places (voids). So, the need to evaluate and enhance the accuracy of these DEMs becomes necessary.

In this study, the accuracy of two global digital elevation models: Shuttle Radar Topography Mission (SRTM1) and ALOS-PALSAR (ALOS-PALSAR Phased Array type L-band Synthetic Aperture Radar) are evaluated by using ground orthometric and GPS heights. Data in two different sites are used: A grid of 239 fixed points cover an area of 18.85 by 12.15 km in Toshka south of Egypt, about 55,000 Fedans and a grid of 2722 points in the southwest of Egypt cover an area of 210 by 120 km, about 6 million Fedans.

The evaluation process was made by comparing the ellipsoidal heights of the two sites with their corresponding values in the used two DEMs and comparing the orthometric heights of the first site points with their

corresponding values in two DEMs.

Then enhancement process made by through four steps. The first step is shifting the model heights using one point in the middle of the area, where the value of this shift is the difference between the ground value and its corresponding value on the used DEM, this shift is applied on the orthometric height values (in the first test area) and once more on the ellipsoidal height values (in both test areas).

The second step is converting the ellipsoidal heights of the used DEM to orthometric values by using (SGG-UGM 2) geoid model instead of the used EGM96 to show the effect of undulation values on the DEMs values. This process was applied to the two DEMs in the test area 1 (Toshka south of Egypt).

The third step is shifting using well distributed five separated points while, every point served an area with 4km radius, and this method was made in two sites (plain and moderate slopes) included in test area 2.

The fourth step is applying first and second order polynomials by using well-distributed five and seven control points respectively (in both sites).

5.2 Conclusions

Based on the computations and the obtained results, the following can be concluded:

- In most study cases, SRTM1 and ALOS-PALSAR both gave reasonable results for the geodetic heights.
- Using DEMs ellipsoidal heights is much better than using their orthometric heights. The averages of the ellipsoidal differences are -

1.87 and -1.47 m after they were -4.15 and -3.75 m as orthometric differences for SRTM1 and ALOS-PALSAR respectively.

- Using recent and accurate geoid model in converting the ellipsoidal heights of the DEM into orthometric heights, improves the DEM performance. The averages of the differences in case of using EGM96 were -4.25 and -3.75 m and in case of using SGG-UGM 2, they were -2.87 and -2.47 m for SRTM1 and ALOS-PALSAR respectively.
- The proposed simple shifting process is very affective in improving the performance of the used GDEM but it doesn't affect its precision. It makes the GDEM surface simply near to the ground surface using one or few ground points. Shifting process improved the average values from -1.87 to 0.02m with SRTM1 and from -1.47 to 0.42m with ALOS-PALSAR in area equals to 25200 km^2.

The results of evaluating the ellipsoidal heights and shifting them using an intermediate point at the different Test areas along the thesis are collected in the following tables and figures.

Table 5.1. Evaluation and improvement (shifting using one point) of SRTM1 ellipsoidal heights over the two-test area cases.

		SRTM1			
Area		(Average) m		(St.dev.) m	
		Evaluation	Improvement	Evaluation	Improvement
Area 1 Km	6.5*5	-2.09	-0.20	2.24	2.23
	12*9	-2.09	-0.20	2.37	2.36
	19*12	-1.87	0.02	2.27	2.27
Area 2	68*49	-4.56	-0.60	3.28	3.28
	143*81	-4.27	-0.31	3.54	3.54

Km	210*120	-4.17	-0.21	3.17	3.17

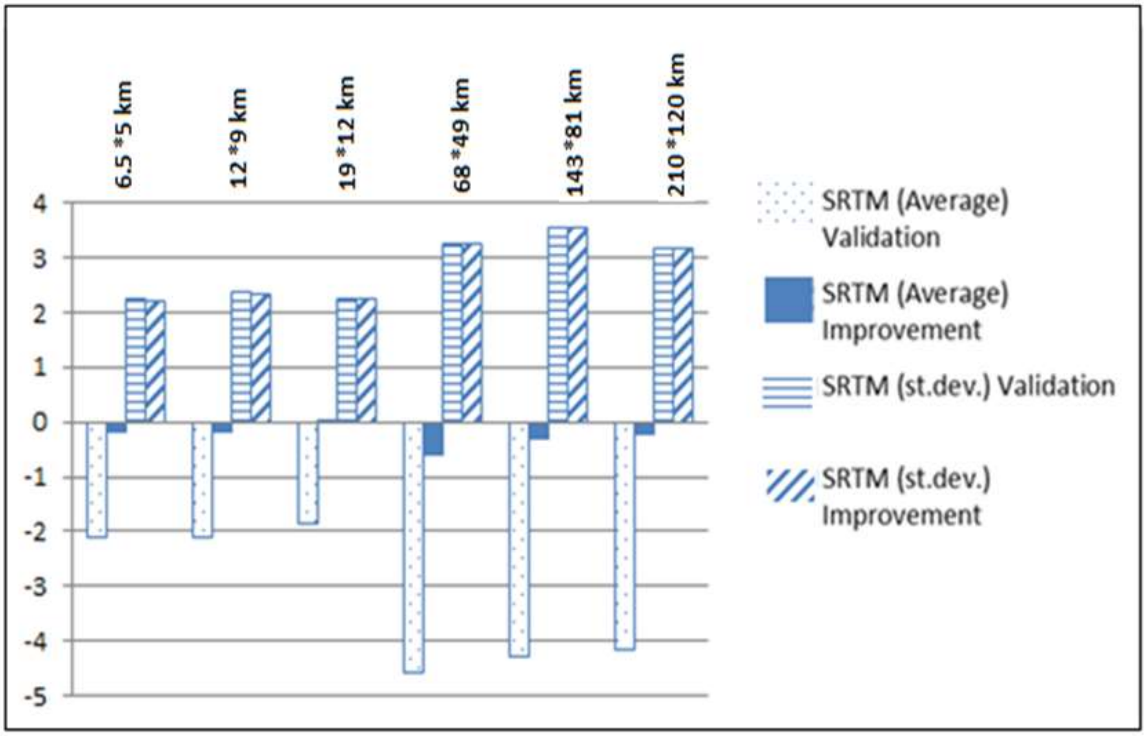

Figure 5.1. Evaluation and improvement (shifting using one point) of SRTM1 ellipsoidal heights over the two-test area cases.

Table 5.2. Evaluation and improvement (shifting using one point) of ALOS-PALSAR ellipsoidal heights over the two test area cases.

		ALOS-PALSAR			
		(Average) m		(St.dev.) m	
	Area	Evaluation	Improvement	Evaluation	Improvement
Area1 Km	6.5*5	-1.68	0.02	2.40	2.39
	12*9	-1.67	0.04	2.49	2.48
	19*12	-1.47	0.42	2.38	2.38

Area2 Km	**68*49**	**-2.64**	**-0.37**	**3.26**	**3.26**
	143*81	**-2.42**	**-0.16**	**3.38**	**3.38**
	210*120	**-2.40**	**-0.13**	**3.14**	**3.14**

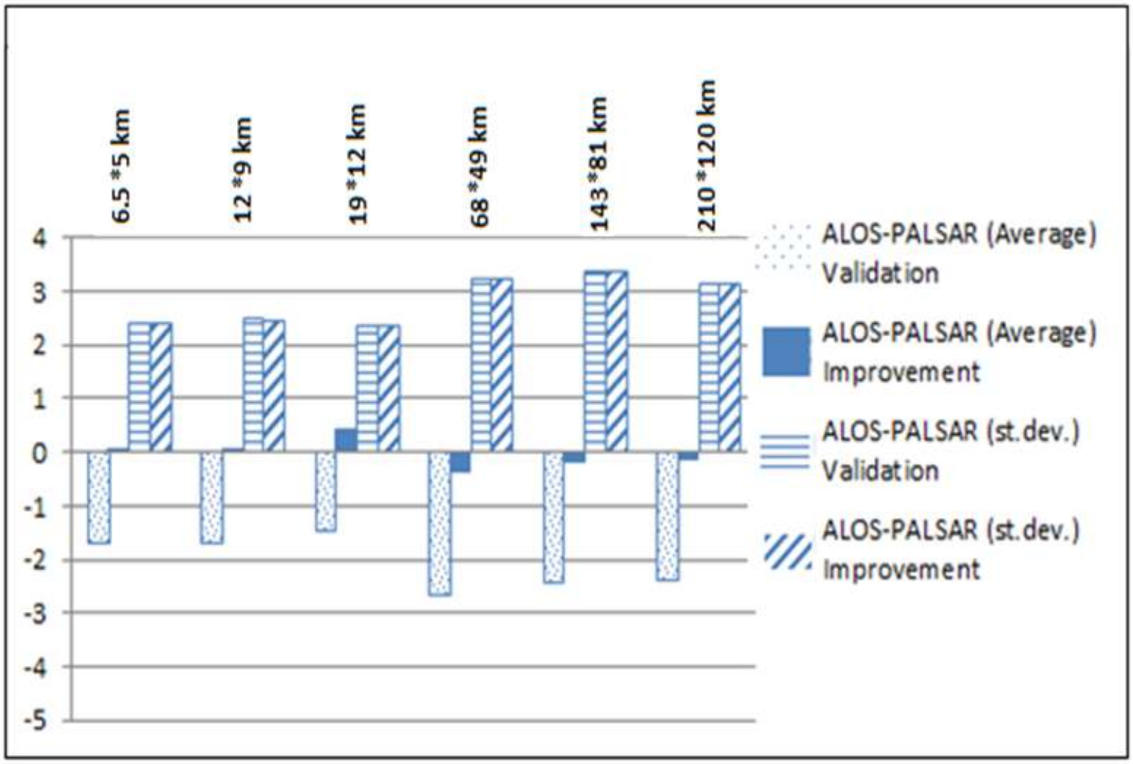

Figure 5.2. Evaluation and improvement (shifting using one point) of ALOS-PALSAR ellipsoidal heights over the two test area cases.

5.3 Recommendations

- It is recommended to use the elevations obtained from SRTM1 because they are more accurate than the elevations obtained from ALOS-PALSAR.
- Because the GDEM points do not accurately reflect the characteristics of the earth surface, it is important to be modified before using them. The simple proposed shifting process can obtain expressive values.

- The choice of the point used in the shifting process depends on the spatial resolution of the global digital elevation models, as this point must fall within the spatial resolution framework.
- It is recommended to observe number of well distributed points in the shifted area to assure that the using one among them in shifting process is not erroneous.
- It is recommended to choose the shifting point in a flat area avoiding the probable model source errors (where the resolution for SRTM1 and ALOS-PALAR is 30 and 12.5 m, respectively).
- It is recommended to adopt a high-accuracy geoid model to obtain precise orthometric heights.
- Future studies have to focus on the error sources of GDEMs and to work on reducing their influences to finally have accurate DEMs.

As future work, it is recommended to develop an approach to correcting the nonlinear errors in global model data. In this regard, the global model data, the new freely available Sentinel-2 multispectral imagery, and GPS reference points can be applied as input in an Artificial Neural Network (ANN) classification model. The probabilities obtained for ANN are then combined based on an Inverse Probability Weighted Interpolation (IPWI) approach to estimate corrected global model elevations.

REFERENCES

Aguilar, M. A., Aguilar, F. J., Sanchez, J. A., Carvajal, F. and Aguera, F., 2007. "Geometric Accuracy Assessment Of QuickBird Basic Imagery Using Different Operational Approaches". Photogrammetric Engineering & Remote Sensing, 73(12), 1321-1332.

Al-Mutairi, M., Alsahli, M., Ibrahim, M., Abou Samra, R., and Gammal, M., 2019. "Spatial enhancement of DEM using interpolation methods: A case study of Kuwait's coastal zones". American Journal of Remote Sensing, 7(1) , 5-12.

Amin, M. M., El-Fatraiy, S. M., and Saba, N. M., 2013. "Accuracy assessment of world DEMs versus local DEM in Egypt". Civil Engineering Research Magazine CERM, 35(3).

Aref, H. and Reinartz, P., 2011. "Accuracy enhancement of ASTER global digital elevation models using ICESat data". Remote Sensing, 3(7), 1323-1343.

Avtar, R., Yunus, A.P., Kraines, S., and Yamamuro, M., 2015. "Evaluation of DEM generation based on interferometric SAR using TanDEM-X data in Tokyo". Physics and Chemistry of the Earth, Parts A/B/C, 83, 166-177.

Borrough, 1998. "Principles of geographical information system". P.A., McDonnell, and A. Rachael Oxford University Press, 356p.

Balasubramanian, A., 2017. "Digital Elevation Model (DEM) in GIS", Centre for Advanced Studies in Earth Science, University of Mysore, Mysore.

Brimicombe, A. (2010). "GIS, environmental modeling and engineering". Second Edition, CRC Press, New York, USA, 361 pp.

Brus, D.J., et al., 1996. "The performance of spatial interpolation methods and choropleth maps to estimate properties at points: A soil survey case study". Envi-
ronmetrics, 7, 1-16. https://doi.org/10.1002/(SICI)1099-
095X(199601)7:13.0.CO;2-Y.

Boissonnat, J., and Cazals, F., 2002. "Natural neighbour coordinates of Points on a surface". Vol. 22, No. (1-3), pp. 185-203.

Butler, J. B., Lane, S. N., & Chandler, J. H. (1998). "Assessment of DEM quality for characterizing surface roughness using close range digital photogrammetry". The Photogrammetric Record, 16(92), 271-291.

Carter, M., Shepherd, J. M., Burian, S., and Jeyachandran, I.,2012. "Integration of lidar data into a coupled mesoscale–land surface model: A theoretical assessment of sensitivity of urban–coastal mesoscale circulations to urban canopy parameters". Journal of Atmospheric and Oceanic Technology, 29 (3): 328–346.

Chang, K. T., 2008. "Introduction to geographic information systems". 9th Edition. Boston: McGraw-Hill.

Collins, F.C. and Bolstad, P.V., 1996. “A comparison of spatial interpolation techniques in temperature estimation”. Proceedings of the 3rd International Conference/Workshop on Integrating GIS and Environmental Modeling, National Center for Geographic Information and Analysis, Santa Barbara, Santa Fe, NM; Santa Bar-bara, CA.

Darve, E., 2000. “The fast multipole method: numerical implementation”. Journal of Computational Physics, 160(1), 195-240.

Darwish, N., Kaiser, M., Koch, M., and Gaber, A., 2021. “Assessing the accuracy of ALOS/PALSAR-2 and Sentinel-1 radar images in estimating the land subsidence of coastal areas: A case study in alexandria city”. Egypt. Remote Sensing, 13(9), 1838.

Dawod, G. and Al-Ghamdi, K., 2017. “Reliability of recent global digital elevation models for geomatics applications in Egypt and Saudi Arabia”. Journal of Geographic Information System, 9(06), 685-698.

Dawod, G. and Amin, A., 2022. “Enhancing vertical accuracy of global digital elevation models for coastal and environmental applications: A case study in Egypt”. American Journal of Geographic Information System 2022, 11(1), 1-8.

Droj, G., 2008. “Improving the accuracy of digital terrain models”. STUDIA UNIV. BABES¸–BOLYAI, INFORMATICA, LIII, 1, 65-72.

El-Ashmawy, N., & Al-Krargy, E., 2022. "Enhancing the GDEMs of Egypt using a surface subtraction approach". Geomatics and Environmental Engineering, 16(3), 57-77.

Elkhrachy. I., 2018. "Vertical accuracy assessment for SRTM and ASTER digital elevation models: A case study of Najran city, Saudi Arabia". Ain Shams Engineering Journal, 9(4), 1807-1817.

El Sayed, M. S., and Ali, A. H., 2016. "Improving the accuracy of the SRTM global DEM using GPS data fusion and regression model". International Journal of Engineering Research, 5(3), 190-196.

FFG Pty Ltd., (2009). "GPS/Gravity Survey, Acquisition and Processing report", Bir Mesaha, Egypt, Fugro Ground Geophysics Pty Ltd. JOB NO. G2449.

Florinsky, I. V. (1998). "Accuracy of local topographic variables derived from digital elevation models". International Journal of Geographical Information Science, 12(1), 47-62.

Grohmann, C., 2006. "Resampling SRTM 03"-data with kriging". GRASS/OSGeo-News, vol. 4.

Hardy, R., 1971. "Multiquadric equations of topography and other irregular surfaces". Journal of geophysical research, 76(8).

Hengl, T., 2009, "A practical guide to geostatistical mapping, http://spatialanalyst.net/book.

Hirt, C (2015). “Digital terrain models”. In: Encyclopedia of Geodesy (Ed. E.W. Grafarend), doi 10.1007/978-3-319-02370-0_31-1, Springer, Berlin, Heidelberg.

Hounam, D., & Werner, M. (1999, September). “The shuttle radar topography mission (SRTM)”. In Proceedings of ISPRS workshop-Sensors and Mapping from Space.

Hussein, Z. E., 2016. “Accuracy evaluation of digital elevation model created
using handheld global positioning system receivers”. Journal of Engineering, 22(6), 137-148.

Hutchinson, J. N., 1995. “Keynote paper: landslide hazard assessment”. In International Symposium on Landslides , pp. 1805-1841.

Ikechukwu, M. N., Ebinne, E., Idorenyin, U., and Raphael, N. I., 2017. Accuracy assessment and comparative analysis of IDW, spline and kriging in spatial interpolation of landform (topography): an experimental study”. Journal of Geographic Information System, 9(3), 354-371.

Isaaks, E. H., and Srivastava, R. M., 1989. “Applied geostatistics”. Oxford University Press. New York, 129(1), 125-126.

Isioye, O. A., Jobin, P., and Youngu, T. T., 2012. “An assessment of digital elevation models (DEMs) from different spatial data sources”. Asian Journal of Engineering, Sciences & Technology, 2(1), 1-17.

Islam, Z., 2011. “A review on water resources management modeling”, University of Alberta.

Jalal, S. J., Musa, T. A., Ameen, T. H., Din, A. H. M., Aris, W. A. W., and Ebrahim, J. M., 2020. “Optimizing the global digital elevation models (GDEMs) and accuracy of derived DEMs from GPS points for Iraq's mountainous areas”. Geodesy and Geodynamics, 11(5), 338-349.

Ledoux, H., and Gold, C., 2005, “An efficient natural neighbor interpolation algorithm for geoscientific modeling”, Developments in spatial data handling. Springer, Berlin, Heidelberg, 97-108.

Linuza,I., 2014. “Accuracy assessment in glacier change analysis”. Master's thesis, Lund University, retrieved from Lund University Publications.

Liu, Z., Zhu, J., Fu, H., Zhou, C., Zuo, T., 2020. “Evaluation of the vertical accuracy of open global DEMs over steep terrain regions using ICESat data: A case study over hunan province”. China. Sensors, 20(17),4865.

Li, L., Bakelants, L., Solana, C., Canters, F., and Kervyn, M., 2018. “Dating lava flows of tropical volcanoes by means of spatial modeling of vegetation recovery”. Earth Surface Processes and Landforms, 43(4), 840-856.

Li, P., Shi, C., Li, Z., Muller, J.-P., Drummond, J., Li, X., Li, T., Li, Y., and Liu, J., 2013. “Evaluation of ASTER GDEM using GPS benchmarks and SRTM in China". International Journal of Remote Sensing, 34(5), 1744-1771.

Maeda, E. E. , 2014. "Downscaling MODIS LST in the East African mountains using elevation gradient and land-cover information". International Journal of Remote Sensing, 35(9), 3094-3108.

Manune, D.F., 2007. "Digital elevation model". Technologies and Applications: The DEM Users Manual, 2nd ed.; American Society for Photogrammetry and Remote Sensing: Bethesda, MD, USA.

Mirza, M., Dawod, G., and Al-Ghamdi, K., 2011. "Accuracy and relevance of digital elevation models for geomatics applications-A case study of Makkah
municipality". Saudi Arabia. International Journal of Geomatics and Geosciences, 1(4), 803.

Mitas, L. and Mitasova, H., 2005. "Spatial Interpolation". In: Longley, P.A., Goodchild, M.F., Maguire, D.J. and Rhind, D.W., Eds., Geographic Information Systems: Principles, Techniques, Management and Applications, 2nd Edition, Vol. 1, Part 2, Chapter 34. www.geos.ed.ac.uk/~gisteac/gis_book_abridged/ .

Mohammed, R. K., 2004. "The optimum choice for contouring". Journal of Civil Engineering Research, 1(1).

Mouratidis, A., Briole, P., and Katsambalos, K., 2010. "SRTM 3″ DEM (versions 1, 2, 3, 4) validation by means of extensive kinematic GPS measurements: a case study from North Greece", International Journal of Remote Sensing, 31(23), 6205–6222.

Mukherjee, S., Joshi, P. K., Mukherjee, S., Ghosh, A., Garg, R. D., and Mukhopadhyay, A., 2013. "Evaluation of vertical accuracy of open source Digital Elevation Model (DEM)". International Journal of Applied Earth Observation and Geoinformation, 21, 205-217.

Nagarajan, K., Narwade, R., Ashwini, P., Panhalkar, S., Kulkarni, V., and Hingmire, A., 2022. "Employing Digital Elevation Model (DEM) for floodplain mapping with applications of HEC-HMS, HEC-RAS, and ArcGIS : A review". Journal of Remote Sensing and ArcGIS, 13(2), 1-16.

Orejuela, I., Gonzalez, C., Guerra, X., Mora, E., and Toulkeridis, T., 2021. "Geoid undulation modeling through the Cokriging method - A case study of Guayaquil, Ecuador". Geodesy and Geodynamics, No. 12, pp. 356-367.

Ouerghi, S., ELsheikh, R. F. A., Achour, H., & Bouazi, S., 2015. "Evaluation and validation of recent freely-available ASTER-GDEM V. 2, SRTM V. 4.1 and the DEM derived from topographical map over SW Grombalia (test area) in North East of Tunisia". Journal of Geographic Information System, 7(03), 266.

Pan, R. and Skala, V., 2011. "A two-level approach to implicit surface modeling with compactly supported radial basis functions". Engineering with computers, 27(3), 299-207.

Pulighe, G., and Fava, F., 2013. “DEM extraction from archive aerial photos: Accuracy assessment in areas of complex topography”. European Journal of Remote Sensing, 46(1), 363-378.

Rabah, M., El-Hattab, A. and Abdallah, M., 2017. “Assessment of the most recent satellite based digital elevation models of Egypt”. NRIAG Journal of Astronomy and Geophysics, 6(2), 326-335.

Ripley, B.D., 1981. “Spatial Statistics”. John Wiley & Sons, New York, 252. https://doi.org/10.1002/0471725218.

Robinson, T. P., and Metternicht, G., 2006. “Testing the performance of spatial interpolation techniques for mapping soil properties”. Computers and electronics in agriculture, 50(2), 97-108.

Saati, A., Arefi, H., Schmitt, M., and Stilla, U., 2011. “Statistically robust detection and evaluation of errors in DTMs”. Urban Remote Sensing Event (JURSE), 2011 Joint , vol., no., pp.305-308, 11-13 April 2011, doi: 10.1109/JURSE.2011.5764780.

Sefercik, U. G., & Ozendi, M., 2013. “Comprehensive comparison of VHR 3D spatial data acquired from IKONOS and TerraSAR-X imagery”. Advances in Space Research, 52(9), 1655-1667.

Setiyoko, A., 2013. “Analysis of spatial interpolation techniques for DEM generation using IRS-1C data”. In 34th Asian Conference on Remote Sensing 2013, ACRS 2013 (Vol. 2, pp. 789-794).

Skala, V., Pan, R, and Nedved, O., 2014. "Making 3D replicas using a flatbed scanner and a 3D printer". International Conference on Computational Science and Its Applications, pp. 76-86.

Uhlir, K. and Skala, V., 2005. "Reconstruction of damaged images using radial basis functions". 13th European Signal Processing ,pp. 1-4.

Van Niel, K. P., and Austin, M. P., 2007. "Predictive vegetation modeling for conservation: Impact of error propagation from digital elevation data". Ecological Applications, 17(1), 266-280.

Wahab, M. A., 2017. "Interpolation and extrapolation". In Proc. Topics Syst. Eng. Winter Term,Vol. 17, pp. 1-6.

Watson, D.F., 1992. "Contouring: A guide to the analysis and display of spatial data". pergamon, Oxford.

Webster, R. and Oliver, M., 2001. "Geo-statistics for Environmental Scientists". John Wiley & Sons, Ltd., Chichester, 271.

Wendland, H., 2006. "Computational aspects of radial basis function approximation". Studies in Computational Mathematics , Vol. 12, pp. 231-256.

Whittingham, M. J., Stephens, P. A., Bradbury, R. B., and Freckleton, R. P., 2006. "Why do we still use stepwise modelling in ecology and behaviour?". Journal of animal ecology, 75(5), 1182-1189.

Wu, Y. H., & Hung, M. C., 2016. "Comparison of spatial interpolation techniques using visualization and quantitative assessment". Applications of spatial statistics, 17-34.

Yang, C. S., Kao, S. P., Lee, F. B., and Hung, P. S., 2004. "Twelve different interpolation methods: A case study of Surfer 8.0". Proceedings of the XXth ISPRS Congress. Vol. 35.

Yang, X., Li, L., Chen, L., Chen, L., & Shen, Z., 2018. "Improving ASTER GDEM accuracy using land use-based linear regression methods: A case study of Lianyungang, East China". ISPRS International Journal of Geo-information, 7(4), 145.

Zapletal, J., Vaněček, P., and Skala, V., 2009. "RBF-based image restoration utilising auxiliary points". Computer Graphics International Conference , pp. 39-43.

Zhou, Q.,Lees, B., and Tang, G., 2008. "Advances in digital terrain analysis", Springer – Verlag Berlin Heidelberg.

Zhu, K., Cui, Z., Jiang, B., Yang, G., Chen, Z., Meng, Q., and Yao, Y., 2013. "A DEM-based residual kriging model for estimating ground water levels within a large-scale domain: A study for the Fuyang River Basin". Clean Technologies and Environmental Policy, 15(4), 687-698.

Websites

https://asf.alaska.edu/data-sets/sar-data-sets/alos-palsar/alos-palsar-about/.

https://asf.alaska.edu/data-sets/derived-data-sets/alos-palsar-rtc/alos-palsar-radiometric-terrain-correction/

https://asf.alaska.edu/wp-content/uploads/2022/09/alos_userhb_en.pdf.

https://asf.alaska.edu/information/palsar-rtc-dem-information/.

https://csm.fresnostate.edu/ees/documents/facstaff/wang/gis200/lecture-notes/gis/chap15.pdf .

https://desktop.arcgis.com/en/arcmap/10.3/tools/3d-analyst-toolbox/how-kriging-works.htm.

https://en.unesco.org/sites/default/files/ukzn_dem_lecture_for_uploa

https://en.wikipedia.org/wiki/Digital_elevation_model.

https://en.wikipedia.org/wiki/Advanced_Spaceborne_Thermal_Emission_and_Reflection_Radiometer.

https://geodetics.com/dem-dsm-dtm-digital-elevation-models

https://gisresources.com/giswatershedwatershed-analysis

https://lpdaac.usgs.gov/documents/262/ASTER_User_Handbook_v2.pdf.

https://makoj.com/blog/2018/april/contours-dem/ .

Newton's Interpolation Methods (nitk.ac.in).

https://pubs.usgs.gov/tm/11b4/pdf/tm11-B4.pdf .

https://www.asprs.org/a/society/committees/lidar/Downloads/Vertical_Accuracy_Reporting_for_Lidar_Data.pdf.

https://www.cs.uaf.edu/~olawlor/ref/asf/sar_equations_2006_08_17.pdf.

https://www.dlr.de/hr/en/desktopdefault.aspx/tabid-8113/14171_read-35852/.

https://www.google.com/url?sa=i&url=http%3A%2F%2Fvterrain.org%2FElevation%2FSRTM%2F&psig=AOvVaw1v-ZHMG1wwkOAwRTwqN66F&ust=1676580917540000&source=images&cd=vfe&ved=0CA4QjhxqFwoTCPiu3Ii5mP0CFQAAAAAdAAAAABBS.

https://gisresources.com/types-interpolation-methods_3.

https://www.iso.org/standard/50461.html.

https://www.nasa.gov/missions.

http://www.terrainmap.com/rm19.html.

https://www.usgs.gov/centers/eros.

https://www.usgs.gov/centers/eros/science/usgs-eros-archive-digital-elevation-shuttle-radar-topography-mission-srtm.

http://www2.jpl.nasa.gov/srtm/.

ملخص البحث:

يعتبر تمثيل تضاريس سطح الأرض ضروريًا في العديد من التطبيقات والاستخدامات ؛ للقيام بذلك ، سنحتاج إلى وقت طويل وجهود كبيرة لتحقيق ذلك من خلال الأجهزة المساحية الأرضية. ولكن استخدام الاقمارالصناعية فى هذا المجال جعل تمثيل سطح الأرض سهلًا ويوفر الوقت والجهد. لسوء الحظ ، فإن المشكلة في هذه الطريقة هي الدقة المنخفضة في العديد من الأماكن وفقًا لطبيعة سطح الأرض وغياب البيانات في أماكن أخرى (الفراغات). لذلك ، فإن الحاجة إلى تقييم وتعزيز الدقة أصبحت ضرورية.

في هذه الدراسة ، تم تقييم دقة نموذجين عالميين للارتفاع الرقمي: Shuttle Radar Topography Mission (SRTM1) و ALOS Phased Array type L-band Synthetic Aperture Radar (ALOS PALSAR) وذلك عن طريق استخدام ارتفاعات أرضيه (orthometric heights) و ارتفاعات مقاسة بنظام تحديد المواقع العالمي (GPS). تم استخدام البيانات في موقعين مختلفين: شبكة ثوابت مكونة من 239 نقطة ثابتة تغطي مساحة 18.85 × 12.15 كم في توشكى جنوب مصر (حوالي 55000 فدان) وشبكة من 2722 نقطة في جنوب غرب مصر تغطي مساحة 210 × 120 كم (حوالي 6 ملايين فدان).

تم إجراء عملية التقييم بمقارنة الارتفاعات (orthometric heights) لنقاط الموقعين مع القيم المقابلة لها في DEMs المستخدمة ومقارنة الارتفاعات (ellipsoidal heights) لنقاط الموقع الأول مع القيم المقابلة لها في اثنين من DEMs.

ثم تتم عملية التحسين من خلال اربع خطوات:

الخطوة الأولى هي تحويل الارتفاعات (ellipsoidal heights) لل DEM المستخدم إلى قيم (orthometric heights) باستخدام نموذج (SGG-UGM-2) الجيود بدلاً من EGM96 المستخدم لإظهار تأثير قيم ال undulations على قيم ال DEM. تم تطبيق هذه العملية على اثنين من ال GDEMs في الموقعين.

الخطوة الثانية هي تغيير (ازاحة) ارتفاعات النموذج باستخدام نقطة واحدة في منتصف المنطقة ، حيث تكون قيمة هذا التحول هي الفرق بين القيمة الأرضية والقيمة المقابلة لها على DEM المستخدم ، ويتم تطبيق هذا التحول على قيم الارتفاعات (orthometric heights(EGM96 and SGGUGM-2)) في الموقع الأول. ومرة أخرى على قيم الارتفاع (ellipsoidal heights) في كلا الموقعين.

الخطوة الثالثة هي التحول باستخدام خمس نقاط موزعة بشكل جيد حيث تغطي كل نقطة نصف قطر 4km وتستخدم كل نقطة منفردة بازاحة المساحة التى تقوم بتغطيتها.وتم استخدام هذه الطريقة علي منطقتين فرعيتين من الموقع الثاني احداهما مستوية والاخري معتدلة التضاريس حيث كل منهما تغطي مساحة (24*24km) . يتم تطبيق هذا التحول على قيم الارتفاع (ellipsoidal heights).

الخطوة الرابعة هي استخدام معادله كثيرات الحدود من الدرجه الأولي والثانية باستخدام خمس نقاط موزعه توزيع جيد في حاله استخدام معادلة كثيرات الحدود من الدرجة الأولي واستخدام سبع نقاط موزعة جيدا في حالة استخدام كثيرات الحدود من الدرجة الثانية علي قيم الارتفاع (ellipsoidal heights)،وقد تم تطبيق هذه الطريقة على الموقع الأول بأكمله، وعلى منطقتين فرعيتين من الموقع الثاني احداهما مستوية والاخري معتدلة التضاريس حيث كل منهما تغطي مساحة (24*24km) ومن ثم مقارنة النتائج مع نتائج الخطوة الثالثة. قد أثبتت النتائج أن نموذج الأرتفاع الرقمي SRTM1 و ALOS-PALSAR قد أعطوا نتائج معقولة عند استخدام الارتفاعات الجيوديسية في معظم حالات الدراسة وأنه من الأفضل التعامل مع قيم الأرتفاعات(ellipsoidal heights) الخاصة بنماذج الارتفاعات الرقمية العالمية (GDEMS) واوضحت أيضا أن الازاحة باستخدام نقطة واحدة تعطي أفضل نتائج من بين الطرق الأخرى المعروضة فى هذه الرسالة.

محتويات البحث:

تقدم هذه الرسالة نظرة عامة موجزة عن عدة أنواع من النماذج الرقمية ، ودقتها المكانيه ، وتقنيات الاستيفاء ، والتقنيات المختلفة لتقييم وتعزيز دقة نماذج الارتفاع الرقمية العالمية المستخدمة على نطاق واسع. تتكون هذه الرسالة من خمسة فصول.

في الفصل الأول ، يتم تقديم الدافع ، وبيان المشكلة ، والأهداف ، والدراسات السابقة ، ونظرة عامة على هيكل الرسالة.

يتم تحديد النماذج الرقمية الثلاثة ، السطح ، والارتفاع ، والتضاريس في الفصل الثاني. ثم يتم تحديد تطبيقات DEMs. يصف الفصل أيضًا دقة نماذج DEMs المكانية والرأسية. يتم توضيح مصادر البيانات المختلفة المطلوبة لإنشاء DEM. أخيرًا ، تم وصف عدد من مهام الأقمار الصناعية التي تم استخدامها وطريقة حصولها علي بيانات الارتفاعات لسطح الأرض ومصادر الأخطاء ، والنماذج العالمية الناتجة.

يتم تناول مختلف الموضوعات المتعلقة بال interpolation في الفصل الثالث. وهو يصف إجراء interpolation ، ويسرد طرق interpolation المختلفة ، ويصف الأشكال المختلفة لل interpolation المكاني. هناك شرح لتقنيات إنشاء DEM المختلفة. جنبا إلى جنب مع تقييم دقة DEMs ، يتم تقديم دور تقنيات interpolation في تعزيز خصائص ال DEMs.

تم وصف البيانات التي تم استخدامها والمنهجية التي تم استخدامها بإيجاز في الفصل الرابع لدعم أهداف البحث. النتائج التي تم الحصول عليها وتحليلها موضحة في الفصل.

يقدم الفصل الخامس استنتاجات لتقييم وتحسين أداء نماذج الارتفاع الرقمي العالمية. يتضمن هذا الفصل أيضًا بعض التوصيات فى مجال البحث والتعليقات النهائية في المستقبل.

جامعة بنها
كلية الهندسة بشبرا
قسم هندسة الجيوماتكس

تقرير جماعى مقدم من لجنة الحكم و المناقشة

عن رسالة الماجستير

المقدمة من

المهندسة / امال عاطف عبدالفتاح مرسي أبوسالم
بكالوريوس هندسة المساحة (2016)
جامعة بنها

والمقدمة للقسم تحت عنوان:

"تقييم وتحسين دقة نماذج الارتفاعات الرقمية العالمية"

"Evaluating and Improving the Accuracy of Global Digital Elevation Models"

<u>المشرفين على البحث:</u>

أ.د:أحمد عبدالستار شاكر	أستاذ المساحه والجيوديسيا-كلية الهندسة بشبرا – جامعة بنها
أ.د: عبدالله احمد سعد	أستاذ المساحه والجيوديسيا-كلية الهندسة بشبرا – جامعة بنها
د: شمس الدين محمد سعد	مدرس المساحه والجيوديسيا-كلية الهندسة بشبرا – جامعة بنها

<u>مقدمة:</u>

هذا التقرير مقدم بناء على موافقة السيد الأستاذ الدكتور نائب رئيس الجامعة بتاريخ **2023-8-10** باعتماد تشكيل لجنة الحكم و المناقشة على الرسالة المقدمة من المهندس /امال عاطف عبدالفتاح مرسي أبوسالم المسجله لدرجة

ماجستير العلوم بقسم هندسة الجيوماتكس – كلية الهندسة بشبرا – جامعة بنها وذلك للحصول على درجة ماجستير العلوم – قسم هندسة الجيوماتكس - تخصص (الجيوديسيا) من كلية الهندسة بشبرا- جامعة بنها.

و تتكون لجنة الحكم و المناقشة من السادة:

أ.د:أحمد عبدالستار شاكر	أستاذ المساحه والجيوديسيا-كلية الهندسة بشبرا – جامعة بنها
أ.د: محمود النقراشى عثمان	أستاذ المساحه والفوتوجرامترى - كلية الهندسة بنين – جامعة الازهر
أ.د: سعد ذكى بلبل	أستاذ المساحه والجيوديسيا-كلية الهندسة بشبرا – جامعة بنها
أ.د: عبدالله احمد سعد	أستاذ المساحه والجيوديسيا-كلية الهندسة بشبرا – جامعة بنها

و عليـــه

بعد اطلاع اللجنة على الرسالة فقد اجتمعت اللجنة المشكلة بعد فحص الرسالة و مناقشة الباحث فى مناقشة علنية يوم 19-09-2023 وذلك بقاعة إجتماعات مجلس الكلية بمبنى كلية الهندسة بروض الفرج حيث تبين من الأطلاع والمناقشة ما يلى:

الوصف العام للرسالة:

تتكون الرسالة من 89 صفحة باللغة الإنجليزية بالإضافة إلى الملخص العربي ويتكون من 3 صفحات، وتتضمن هذه الرسالة دراسة في تقييم وتحسين دقة نماذج الارتفاعات الرقمية العالمية. وتحتوي الرسالة على عدد (5) فصول بالإضافة إلى قائمة للمراجع وملخص باللغة العربية. وفصول الرسالة الخمسة هي:

الفصل الاول:(introduction)

يحتوي هذا الفصل على نبذة مختصرة عن الدراسات السابقة عن تقييم وتحسين دقة نماذج الرتفاعات الرقمية العالمية ونتائج هذه الدراسات، كما يقدم هذا الفصل أهداف هذه الدراسة وكذلك محتويات الرسالة.

الفصل الثاني:(Digital Elevation Models)
يتناول هذا الفصل كل ما يتعلق بنماذج الارتفاعات الرقمية العالمية من حيث تعريفها وطرق تجميع البيانات اللازمة لانشائها ودقاتها المكانية والراسيه وطرق تقييمها.

الفصل الثالث:(Interpolation and Enhancement Methods)
يتناول هذا الفصل طرق التقدير الحسابى المختلفه وتعريفها والطرق المختلفة لتطبيقها وكيفية استخدامها في تحسيين دقة نماذج الارتفاعات الرقمية العالمية

الفصل الربع:(Data used, Methodology and Results)
يتناول هذا الفصل البيانات المستخدمة في الدراسة والمنهجية المتبعة لتقييم وتحسين دقة نماذج الارتفاعات الرقمية العالمية ومن ثم عرض النتائج التى تم الحصول عليها. في هذه الدراسة تم اختيار نموذجين للارتفاعات الرقمية لتقييمهما وتحسينهما وتم استخدام نقاط ارضية في منطقتين مختلفتيين لاستخدامهما فى عملية التقييم والتحسيين.
تمت عملية التقييم علي مرحلتين: الاولى مقارنة الارتفاعات الارثومترية الخاصة بنماذج الارتفاعات الرقمية بالبيانات الارثومترية الارضية والثانية من خلال مقارنة الارتفاعات الجيوديسية الخاصة بنماذج الارتفاعات الرقمية بالبيانات الجيوديسية الارضية عند نفس النقاط.
تمت عملية التحسين علي اربع خطوات: الاولي هي دراسة تاثيراستبدال نموذج جيود باخروالثانية هي عباره عن ازاحة الارتفاعات الارثومترية والجيوديسية الخاصة بنماذج الارتفاعات الرقمية والثالثه هي عبارة عن الازاحة باستخدام خمس نقاط للارتفاعات الجيوديسية لهذه النماذج في منطقتين مختلفتين داخل الموقع الثاني حيث ان مساحة كل منهم24*24 km والخطوة الرابعة هى استخدام كثيرات الحدود من الدرجة الاولي والثانية.

الفصل الخامس:(Conclusions and Recommendations)
في هذا الفصل، يتم استعراض ملخص للدراسات التي أجريت في الرسالة الحالية بالإضافة إلى تحديد الاستنتاجات الأساسية. وأخيرًا، تم تقديم المزيد من التطورات التي يمكن إجراؤها بناءًا على نتائج العمل البحثي. وبناء عليه فإن الباحثة قد قام باستعراض الموضوع بشكل مميز وقام أيضًا بمناقشة وتفسير النتائج وعرضها من خلال عدة رسومات وإجراء المقارنات بينها. كما قام الباحثة باستخدام مراجع علمية حديثة.

الخلاصة و التوصية

مما سبق تبين أن الباحثة قامت بعرض وشرح موضوع الرسالة بطريقة سليمة وواضحة مستعينة بالجداول والرسم البياني والصور التي ساعدت على توضيح الغرض من الدراسة كما أجابت الباحثة علي استفسارات لجنة الحكم والمناقشة بطريقة علمية سليمة وتوصلت إلى نتائج قيمة ومتميزة في الهندسة المساحية في تخصص الجيوديسا. والرسالة مبنية على أسس علمية سليمة ومكتوبة بلغة إنجليزية مقبولة في مجملها وذات قيمة علمية متميزة في مجال الهندسة المساحية.

ولقد قامت اللجنة بمناقشة الباحثة بمقر كلية الهندسة بشبرا – جامعة بنها، وذلك يوم الثلاثاء الموافق 2023/09/19، والتي قدمت عرضاً جيداً لموضوع البحث وأجابت على أسئلة واستفسارات اللجنة. لذا نوصى بمنحها درجة ماجستير العلوم فى الهندسة المساحية (تخصص الجيوديسيا) من قسم هندسة الجيوماتكس – كلية الهندسة بشبرا – جامعة بنها.

لجنة الحكم والمناقشة		**التوقيع**
ا.د:أحمد عبدالستار شاكر	أستاذ المساحه والجيوديسيا-كلية الهندسة بشبرا – جامعة بنها	....
ا.د: محمود النقراشى عثمان	أستاذ المساحه والفوتوجرامترى - كلية الهندسة بنين – جامعة الازهر	....
ا.د: سعد ذكى بلبل	أستاذ المساحه والجيوديسيا-كلية الهندسة بشبرا – جامعة بنها	....
أ.د: عبدالله احمد سعد	أستاذ المساحه والجيوديسيا-كلية الهندسة بشبرا – جامعة بنها	....

كلية الهندسة بشبرا

FACULTY OF ENGINEERING AT SHOUBRA

القبول النهائي للرسالة

تقييم وتحسين دقة نماذج الارتفاعات الرقمية العالمية

رسالة مقدمة كجزء من متطلبات الحصول على درجة الماجستير في هندسة المساحة

مقدمة من

م/ امال عاطف عبدالفتاح مرسي ابوسالم

بكالوريوس هندسة المساحة (2016)

وقد تمت مناقشة الرسالة والتوصية بالموافقة على منح درجة ماجستير العلوم الهندسية في الهندسة المساحية تخصص الجيوديسيا.

أعضاء لجنة الاشراف

ا.د/ احمد عبدالستار شاكر — التوقيع:

أستاذ المساحة والجيوديسيا- كلية الهندسة بشبرا- جامعة بنها

ا.د/ عبدالله احمد سعد — التوقيع:

أستاذ المساحة والجيوديسيا- كلية الهندسة بشبرا- جامعة بنها

د/ شمس الدين محمد سعد — التوقيع:

مدرس المساحة والجيوديسيا- كلية الهندسة بشبرا- جامعة بنها

تاريخ المناقشة: 2023/09/19

كلية الهندسة بشبرا

FACULTY OF ENGINEERING AT SHOUBRA

القبول النهائي للرسالة

تقييم وتحسين دقة نماذج الارتفاعات الرقمية العالمية

رسالة مقدمة كجزء من متطلبات الحصول على درجة الماجستير فى هندسة المساحة

مقدمة من

م/ امال عاطف عبدالفتاح مرسي ابوسالم

بكالوريوس هندسة المساحة (2016)

وقد تمت مناقشة الرسالة والتوصية بالموافقة على منح درجة ماجستير العلوم الهندسية في الهندسة المساحية تخصص الجيوديسيا.

أعضاء لجنة الحكم والمناقشة

ا.د/ أحمد عبدالستار شاكر — التوقيع:..................

أستاذ المساحة والجيوديسيا- كلية الهندسة بشبرا- جامعة بنها

ا.د/ محمود النقراشي عثمان — التوقيع:..................

أستاذ المساحة والفوتوجرامترى- كلية الهندسة- جامعة الأزهر

ا.د/ سعد ذكى بلبل — التوقيع:..................

أستاذ المساحة والجيوديسيا- كلية الهندسة بشبرا- جامعة بنها

ا.د/ عبدالله أحمد سعد — التوقيع:..................

أستاذ المساحة والجيوديسيا- كلية الهندسة بشبرا- جامعة بنها

تاريخ المناقشة: 2023/09/19

جامعة بنـها
كليـة الـهندسة بشبرا
قسم هندسة الجيومـاتكس

تقييم وتحسين دقة نماذج الارتفاعات الرقمية العالمية

رسالة مقدمة كجزء من متطلبات الحصول على درجة الماجستير فى هندسة المساحة

مقدمة من

م/ امال عاطف عبدالفتاح مرسي ابوسالم

بكالوريوس هندسة المساحة (2016)

اشراف

ا.د/ أحمد عبدالستار شاكر
أستاذ المساحة والجيوديسيا
كلية الهندسة بشبرا
جامعة بنها

ا.د/ عبدالله أحمد سعد
أستاذ المساحة والجيوديسيا
كلية الهندسة بشبرا
جامعة بنها

د/ شمس الدين محمد سعد
مدرس المساحة والجيوديسيا
كلية الهندسة بشبرا
جامعة بنها

القاهرة – جمهورية مصر العربية

2023